

AD-A 114 543

TECHNICAL  
LIBRARY

AD-A 114 543

AD

MEMORANDUM REPORT ARBRL-MR-03155

NUMERICAL SIMULATION OF YAWED  
ROD IMPACTS

B. E. Ringers

February 1982



US ARMY ARMAMENT RESEARCH AND DEVELOPMENT COMMAND  
BALLISTIC RESEARCH LABORATORY  
ABERDEEN PROVING GROUND, MARYLAND

Approved for public release; distribution unlimited.

DTIC QUALITY INSPECTED 3

Destroy this report when it is no longer needed.  
Do not return it to the originator.

Secondary distribution of this report by originating  
or sponsoring activity is prohibited.

Additional copies of this report may be obtained  
from the National Technical Information Service,  
U.S. Department of Commerce, Springfield, Virginia  
22161.

The findings in this report are not to be construed as  
an official Department of the Army position, unless  
so designated by other authorized documents.

*The use of trade names or manufacturers' names in this report  
does not constitute indorsement of any commercial product.*

UNCLASSIFIED

SECURITY CLASSIFICATION OF THIS PAGE (When Date Entered)

| REPORT DOCUMENTATION PAGE  |                       | READ INSTRUCTIONS<br>BEFORE COMPLETING FORM                                    |
|--|-----------------------|--|
| 1. REPORT NUMBER<br>Memorandum Report ARBRL-MR- 03155  | 2. GOVT ACCESSION NO. | 3. RECIPIENT'S CATALOG NUMBER  |
| 4. TITLE (and Subtitle)<br>NUMERICAL SIMULATION OF YAWED ROD IMPACTS   |                       | 5. TYPE OF REPORT & PERIOD COVERED<br>Final                                    |
| 7. AUTHOR(s)<br>B. E. RINGERS  |                       | 6. PERFORMING ORG. REPORT NUMBER   |
| 9. PERFORMING ORGANIZATION NAME AND ADDRESS<br>US Army Ballistic Research Laboratory<br>ATTN: DRDAR-BLT<br>Aberdeen Proving Ground, MD 21005   |                       | 8. CONTRACT OR GRANT NUMBER(s)   |
| 11. CONTROLLING OFFICE NAME AND ADDRESS<br>US Army Armament Research & Development Command<br>US Army Ballistic Research Laboratory (DRDAR-BL)<br>Aberdeen Proving Ground, MD 21005  |                       | 10. PROGRAM ELEMENT, PROJECT, TASK<br>AREA & WORK UNIT NUMBERS<br>1L162618AH80 |
| 14. MONITORING AGENCY NAME & ADDRESS (if different from Controlling Office)  |                       | 12. REPORT DATE<br>February 1982   |
|  |                       | 13. NUMBER OF PAGES<br>55  |
|  |                       | 15. SECURITY CLASS. (of this report)<br>UNCLASSIFIED                           |
| 16. DISTRIBUTION STATEMENT (of this Report)<br><br>Approved for public release; distribution unlimited.  |                       | 15e. DECLASSIFICATION/DOWNGRADING<br>SCHEDULE                                  |
| 17. DISTRIBUTION STATEMENT (of the abstract entered in Block 20, if different from Report)   |                       |  |
| 18. SUPPLEMENTARY NOTES  |                       |  |
| 19. KEY WORDS (Continue on reverse side if necessary and identify by block number)<br>Hydrodynamic Lagrangian Code<br>Finite Element<br>KE Penetration<br>Numerical Simulation<br>Terminal Ballistics  |                       |  |
| 20. ABSTRACT (Continue on reverse side if necessary and identify by block number) (mph)<br>Numerical simulations using a three-dimensional, Lagrangian, finite element, elastic-plastic wave propagation code, EPIC-3 were performed of yawed and nonyawed long rod penetrators impacting single targets. Comparison with experimental results, specifically, residual penetrator velocity and length, plug shape, velocity and mass, as well as a discussion of plugging simulation problems are presented. |                       |  |

DD FORM 1 JAN 73 1473

EDITION OF 1 NOV 65 IS OBSOLETE

UNCLASSIFIED

SECURITY CLASSIFICATION OF THIS PAGE (When Date Entered)

## TABLE OF CONTENTS

|   | Page |
|---|------|
| I. INTRODUCTION . . . . .   | 9    |
| II. EXPERIMENTAL PROGRAM . . . . .                                    | 10   |
| III. NUMERICAL SIMULATIONS USING ORIGINAL VERSION OF EPIC-3 . . . . . | 12   |
| IV. NUMERICAL SIMULATION USING REVISED EPIC-3 . . . . .               | 34   |
| V. CONCLUSIONS . . . . .  | 38   |
| APPENDIX A SLIDING SURFACE TREATMENT . . . . .                        | 41   |
| APPENDIX B DEFINITIONS . . . . .                                      | 45   |
| REFERENCES . . . . .  | 53   |
| DISTRIBUTION . . . . .  | 55   |

LIST OF ILLUSTRATIONS

| Figure |  | Page |
|--------|--|------|
| 1      | Radiographs of Nonyawed Round . . . . .  | 13   |
| 2      | Radiographs of Yawed Round . . . . .   | 14   |
| 3      | Experimental Setup . . . . .   | 15   |
| 4      | Comparative Gridding Sizes   |      |
|        | A. 3 Ring Gridding . . . . .   | 17   |
|        | B. 5 Ring Gridding . . . . .   | 18   |
| 5      | Case A: Nonyawed Penetrator, Coarse Gridding . . . . .   | 21   |
| 6      | Case B: Nonyawed Penetrator, Fine Gridding . . . . .   | 22   |
| 7      | Case C: Yawed Penetrator, Fine Gridding . . . . .  | 24   |
| 8      | Case D: Isometric Deformation Plots of Nonyawed<br>Penetrator at Four Time Steps . . . . .                                     | 26   |
| 9      | Case D   |      |
|        | A. Cross-Sectional Deformation Plot of Release of Plug. . . . .  | 27   |
|        | B. Isometric Deformation Plot of Release of Plug. . . . .  | 27   |
| 10     | Case D   |      |
|        | A. Cross-Sectional Deformation Plot at 25 $\mu$ s . . . . .  | 28   |
|        | B. Cross-Sectional Deformation Plot at 45 $\mu$ s . . . . .  | 28   |
| 11     | Case E: Isometric Deformation Plot of Yawed Penetrator<br>at Four Time Steps . . . . .   | 30   |
| 12     | Cross-Sectional Deformation Plot of Nonyawed Penetrator<br>at 30 $\mu$ s With $\bar{\epsilon} = 3$ for Total Failure . . . . . | 31   |
| 13     | Case E: Isometric Deformation Plot of Yawed Penetrator<br>at 45 $\mu$ s After Release of the Plug . . . . .                    | 32   |
| 14     | Case E: Cross-Sectional Deformation Plots of Yawed<br>Penetrator at 40 and 45 $\mu$ s . . . . .                                | 33   |

LIST OF ILLUSTRATIONS (cont'd)

| Figure |  | Page |
|--------|--|------|
| 15     | Cross-Sectional Plots of $4^{\circ}$ Yaw Case Using Revised EPIC-3 . . . . . | 37   |
| A1     | Severe Deformation of Thin Target . . . . .                                  | 44   |
| B1     | Coordinate System Depicting Angles $\lambda$ , $\phi$ , and $\theta$ . . . . | 49   |
| B2     | Coordinate System Depicting Yaw Angles $\alpha$ , $\beta$ , and $\delta$ . . | 52   |

LIST OF TABLES

| Table |  | Page |
|-------|--|------|
| 1     | RADIOGRAPHICALLY DETERMINED EXPERIMENTAL RESULTS. . . . .        | 11   |
| 2     | MATERIAL PROPERTIES . . . . .                                    | 20   |
| 3     | EXPERIMENTAL VERSUS SIMULATION RESULTS . . . . .                 | 35   |
| 4     | MATERIAL PROPERTIES FOR 4 <sup>0</sup> YAW COMPUTATION . . . . . | 36   |

## I. INTRODUCTION

It is common knowledge that substantial yaw is detrimental to penetrator performance and that any projectiles can be defeated by some combination of target materials and/or spacing.

With the increased use of long rod kinetic energy penetrators against spaced targets, the ability to accurately simulate yawed impacts against complex target arrays would be of tremendous value. Numerical simulations with computer codes enable us to examine each stage of penetration in detail and it is hoped that the continuing development and sophistication of these codes will aid in determining both the best penetrator-target combination to minimize the effects of possible yaw and conversely, the best spacing and thickness of targets to defeat probable long rod threats.

The purpose of the work described in this paper was to model yawed as well as nonyawed impacts against relatively thin targets where perforation was expected to occur. The EPIC-3<sup>1</sup> Lagrangian finite element computer code, developed by Dr. Gordon R. Johnson of Honeywell, was used for this study. We had added the capability of discarding and/or adding targets so that a spaced target situation could be analyzed. Experiments were performed wherein a 65 gram VIMVAR processed steel rod, length-to-diameter ratio of 10 impacted a double target of 10mm RHA and 22.5mm RHA separated by a 152.4mm air gap at normal incidence. An attempt was made to model two firing situations, one with less than 1° total striking yaw at 830 m/s striking velocity, the other with 6.86° total striking yaw at 840 m/s striking velocity. A numerical simulation was also performed of a 27 g Bearcat rod, length-to-diameter ratio of 10 impacting a single target of 12.5mm RHA at normal incidence with a striking velocity of 927 m/s with a yaw of 4° using a revised version of EPIC-3<sup>2</sup>.

A comparison between experimental and numerical simulation results is presented here as well as a discussion of the variation in failure criteria involved in the numerical simulations and the problems encountered in attempting to model plugging failure, which subsequently prevented

---

*\*Spaced target meaning, in this case, two or more target plates separated by measurable air gap(s).*

<sup>1</sup>Gordon R. Johnson, "EPIC-3 A Computer Program For Elastic-Plastic Impact Calculations in 3 Dimensions", BRL CR 343, July 1977. (AD A043281)

<sup>2</sup>Gordon R. Johnson "Further Development of the EPIC-3 Computer Program For Three-Dimensional Analysis of Intense Impulsive Loading", AFATL-TR-78-81, July 1978.

simulation of the residual penetrator and plug through the air gap and into the second target in the case of the double target situation.

## II. EXPERIMENTAL PROGRAM

The experimental program was conducted primarily to provide data with which to compare the results of the numerical simulation. The intent was to fire a sufficient number of long rod penetrators at varying degrees of striking yaw against a typical double target configuration to provide reliable empirical data.

There were several constraints on the firing situation. To obtain a clear picture of the effect of the first target on the penetrator there had to be sufficient space between the two targets to ascertain the residual rod orientation and velocity before the second target was reached. This precluded using several standard double targets wherein the spacing between plates is less than the length of the rod planned for these shots. A double target is usually composed of a relatively thin target followed by an air gap and a relatively thick target. It was thought that EPIC-3 could handle perforation of thin targets but it cannot handle deep penetration or perforation of thick targets due to the sliding surface treatment in the current versions of EPIC-3. (See Appendix A for a description of the sliding surface treatment.) Therefore the residual velocity of the rod between the plates had to be considerably less than the limit velocity of the second target.

It was decided to attempt two magnitudes of velocities, one near the limit velocity of the first target and one considerably higher but less than the limit velocity of the second target. Normal incidence was considered to be the least complex situation and therefore the best with which to begin yawed impact studies in combination with spaced targets.

Table 1 shows the results of the firing program which consisted of 20 rounds. Only the results of those rounds for which striking and residual velocities were attained are included. A 65g VIMVAR processed steel rod, length-to-diameter ratio of 10, diameter of 10.2mm was fired at normal incidence against a double target of 10mm RHA and 22.5mm RHA separated by a 152.4mm air gap. A velocity of 430 m/s, just above the limit velocity predicted by Lambert's<sup>3</sup> algorithm for the 10mm plate was attempted for rounds 1-13. Such a low velocity presented problems in determining the correct amount of powder for the gun and the corresponding timings for the x-ray flashes so that data for only four rounds was obtained and the residual results for these are questionable in that, except for round 11, the first residual penetrator image was still within the target on the radiographs.

---

<sup>3</sup>J. P. Lambert, "A Residual Velocity Predictive Model for Long Rod Penetrators", ARBRL-MR-02828, September 1977. (AD B027660)

Table 1. Radiographically Determined Experimental Results

| *Round | PRE-IMPACT         |                     |                     |                  | PENETRATOR            |                        |                 |                  |                   |                |                 | POST-IMPACT    |                  |                   |          |           |           |
|--------|--------------------|---------------------|---------------------|------------------|-----------------------|------------------------|-----------------|------------------|-------------------|----------------|-----------------|----------------|------------------|-------------------|----------|-----------|-----------|
|        | Vert Yaw (α) (Deg) | Horiz Yaw (β) (Deg) | Total Yaw (δ) (Deg) | Strkng Vel (m/s) | Vert Yaw Rate (rev/s) | Horiz Yaw Rate (rev/s) | Resid Vel (m/s) | Cone Angle (Deg) | Phase Angle (Deg) | Resid Mass (G) | Resid Leng (CM) | Plug Vel (m/s) | Cone Angle (Deg) | Phase Angle (Deg) | Mass (G) | Leng (CM) | Diam (CM) |
| 4**    | .3                 | -.2                 | .3                  | 474              | -25                   | -                      | 376             | 2                | 335               | 62.25          | 9.73            | 366            | 37               | 120               | 4.43     | .64       | 1.07      |
| 6**    | -.1                | .4                  | .4                  | 434              | 0                     | -                      | 286             | 7                | 70                | 63.57          | 9.94            | 399            | 31               | 98                | 5.63     | .58       | 1.26      |
| 7**    | -.9                | -.8                 | 1.2                 | 426              | -192                  | -                      | 189             | 68               | 117               | 61.22          | 9.57            | 274            | 13               | 266               | 5.45     | .76       | 1.08      |
| 11     | -.4                | .3                  | 4.                  | 427              | -19                   | -13                    | 258             | 17               | 166               | 47.23          | 7.38            | 339            | 14               | 97                | 5.91     | .79       | 1.1       |
| 14     | 1.3                | .7                  | 1.5                 | 820              | 53                    | -16                    | 679             | 2                | 278               | 43.39          | 6.78            | 711            | 4                | 263               | 12.89    | .98       | 1.47      |
| 15     | -.5                | -.9                 | 1.                  | 844              | 123                   | -                      | 706             | -                | -                 | 53.4           | 8.35            | 686            | 2                | 346               | 9.84     | .86       | 1.36      |
| 16     | .17                | .96                 | .97                 | 834              | 14                    | 155                    | 673             | 2                | 104               | 52.21          | 8.16            | 676            | 2                | 228               | 12.17    | .89       | 1.49      |
| 17     | -.7                | 2.2                 | 7.3                 | 854              |                       | 203                    | 560             | -                | -                 | 37.38          | 5.84            | 675            | 40               | 356               | 10.86    | .81       | 1.48      |
| 19     | -.8                | -2.6                | 2.7                 | 845              | 139                   | 472                    | 632             | 8                | 255               | 47.54          | 7.43            | 715            | 12               | 263               | 3.56     | .55       | 1.03      |
| 20     | -5.3               | -4.4                | 6.86                | 841              | 586                   | 521                    | 550             | 23               | 223               | 38.01          | 5.94            | 663            | 6                | 201               | 13.21    | .75       | 1.7       |

\*See Appendix B for definitions of most of these terms.

\*\*Note: Residual measurements for rounds 4-7 can not be considered reliable since the second penetrator image was still within the first target.

Rounds 14-20 attempted a striking velocity of approximately 830 m/s, somewhat lower than the limit velocity predicted by Lambert's algorithm for the second target. Data was successfully recorded for six of these shots and two of these presented extremes and were considered best for an initial attempt at modeling by the code.

Round 16 had less than  $1^\circ$  total yaw (hereinafter referred to as the non-yawed case); the radiographic results are shown in Figure 1. Residual vertical and horizontal yaw rates of 14 rev/s and 155 rev/s were noted for the penetrator. Both penetrator and the resulting plug deviated little from the original line of flight as indicated by the cone angles of  $2^\circ$  for each.

Round 20 had  $6.86^\circ$  total yaw (herein after referred to as the yawed case); the radiographic results are shown in Figure 2. Yaw was imparted by firing the projectile close to the edge of a hole  $11/16''$  in diameter cut in a thin RHA plate and placed in front of the blast shield. (See Figure 3 for the experimental setup.) This situation is not easy to control so does not lend itself to easy replication. The residual vertical and horizontal yaw rates were 586 rev/s and 521 rev/s respectively, much greater than for the nonyawed case and the penetrator deviated considerably from the line of fire as indicated by a cone angle of  $23^\circ$ . The plug in this case had a cone angle of  $6^\circ$ . A distinct bend, toward the far end of the residual rod is noted in the residual radiographs. The far end of the penetrator has broken off and is still in the target at the time the radiograph recorded the event. A third image was also obtained in the side radiograph which shows the penetrator slamming against the second plate. The data available in the radiographs of this round provided an excellent firing situation to simulate numerically, acknowledging the fact that it was not replicated.

It was hoped that the vast difference in the residual results between these cases of 1) essentially no yaw and 2) considerable yaw would be readily reflected in the simulations.

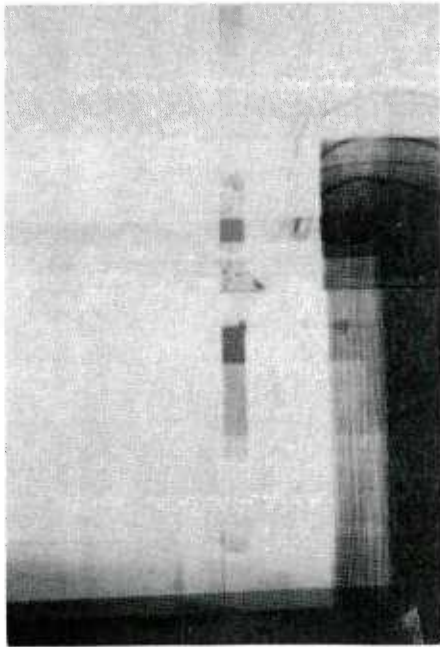
### III. NUMERICAL SIMULATIONS USING ORIGINAL VERSION OF EPIC-3

Numerical simulations of two impact situations were attempted using the original version of EPIC-3. The original version of EPIC-3<sup>1</sup> uses a total-elastic, incremental-plastic formulation and unloading is handled as though the material is rigidly plastic. The revised version<sup>2</sup> uses an incremental elastic-plastic formulation which unloads parallel to the slope of the elastic portion of the stress-strain curve. EPIC-3 had produced good results in comparison with experiment for simulations of yawed impacts of long rods against a single target where the projectile was severely over-matched by the target and no penetration occurred<sup>4</sup> and for oblique impacts

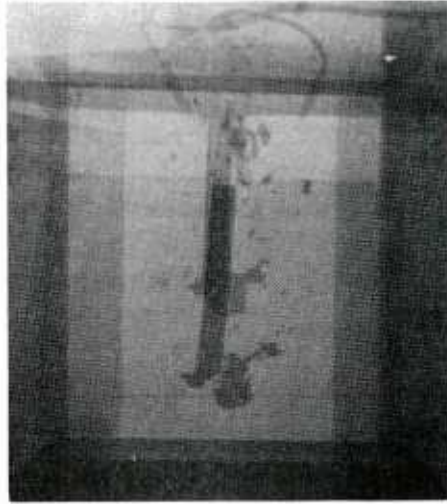
---

<sup>4</sup> J.A. Zukas and B. E. Ringers, "Numerical Simulation of Impact Phenomena", *Proceedings of the 1980 Summer Computer Conference*, AFIPS Press, 1980.

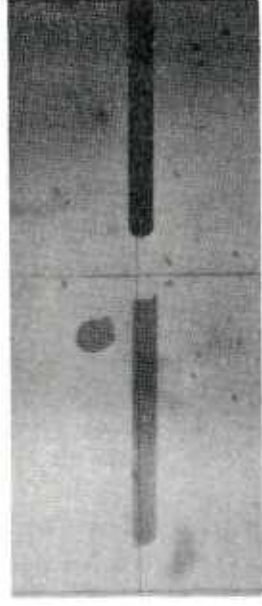
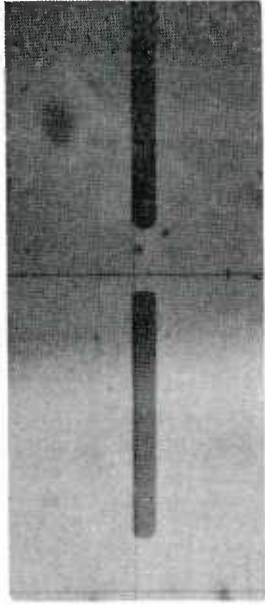
ROUND 16



SIDE



BOTTOM

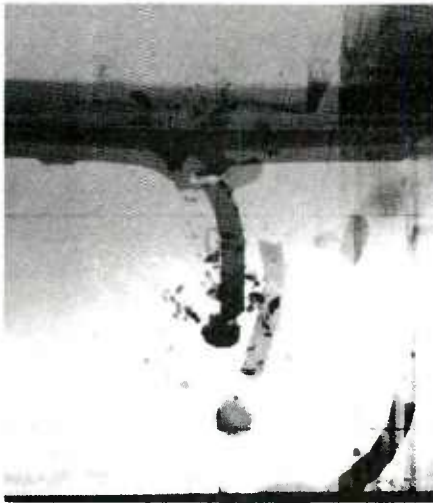


← 2nd TARGET

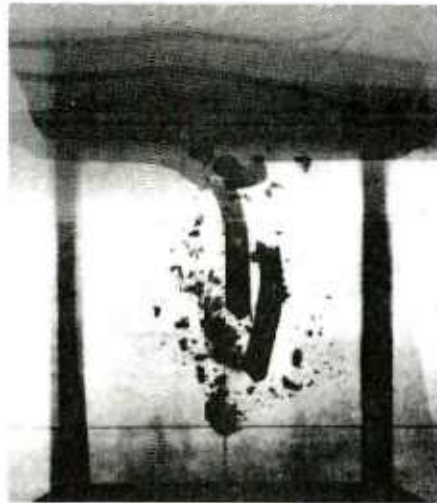
← 1st TARGET

Figure 1. Radiographs of Nonyawed Round

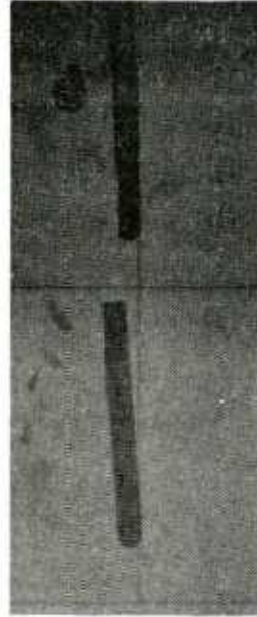
ROUND 20



SIDE



BOTTOM



← 2<sup>nd</sup> TARGET      ← 1<sup>st</sup> TARGET

Figure 2. Radiographs of Yawed Round

# EXPERIMENTAL SETUP

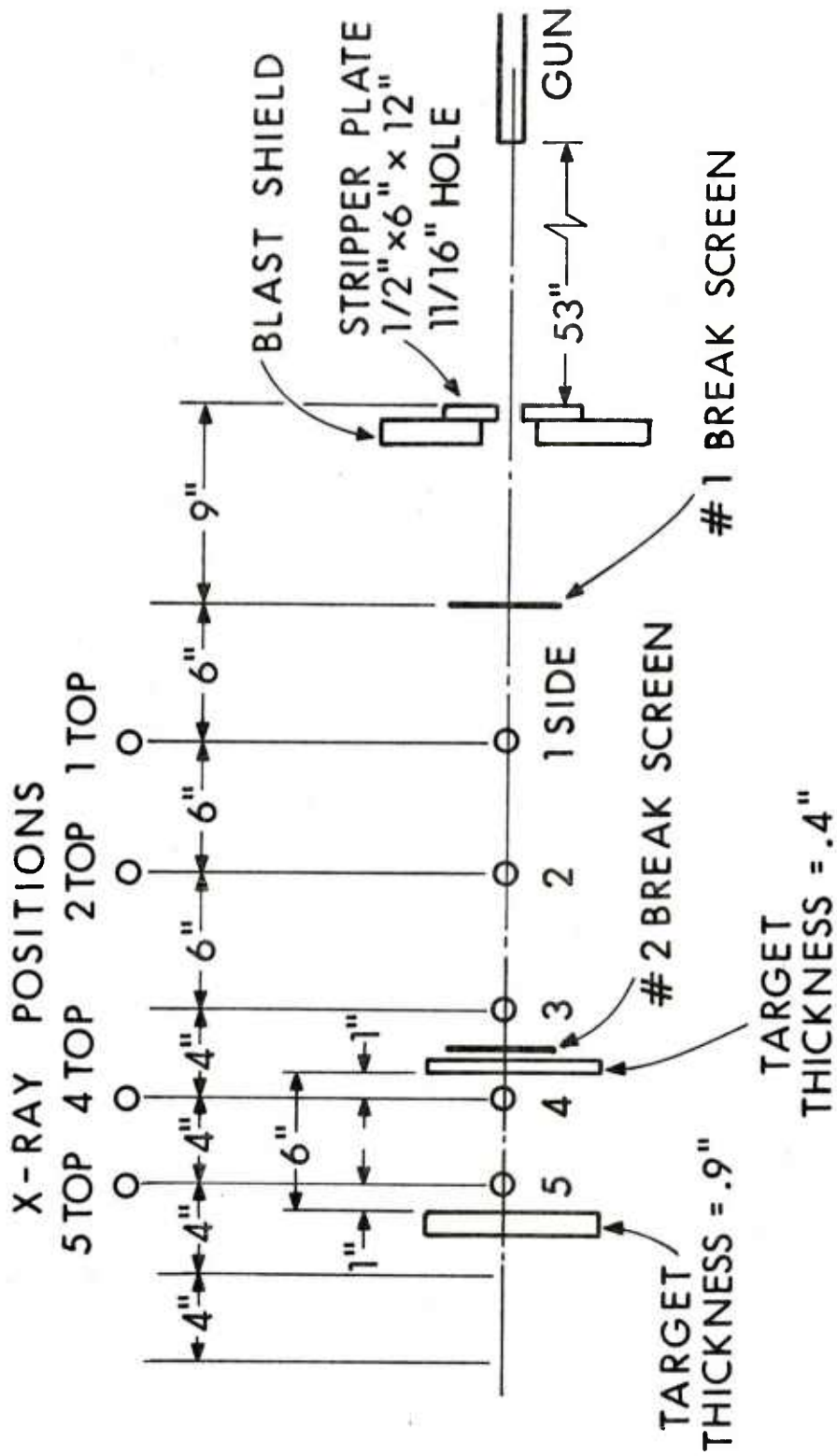


Figure 3. Experimental Setup

12 FEB 79

where the calculation was stopped after partial penetration<sup>5</sup>. It was considered feasible to simulate both nonyawed and yawed impacts against a relatively thin target at velocities which would produce perforation of the target.

Spaced-target impact situations are of substantial interest and two-dimensional simulations of such have been performed only recently by Matuska and Osborn<sup>6</sup>, formerly at Eglin AFB, using an Eulerian code, HULL, and by Bertholf and Kipp<sup>7</sup> at Sandia Labs using CSQ, an Eulerian code, and TOODY, a Lagrangian code, in conjunction with each other.

Since EPIC-3 was amenable to change it was decided to add the capability of discarding and adding targets to the code enabling three-dimensional spaced-target simulations as long as one target could be discarded before another was added.

Accordingly, experiments were performed, (see Section II) and two experimental situations were modeled using EPIC-3; the initial geometry and impact situation being similiar for experiment and calculation.

The following is a discussion of the simulations attempted and the problems encountered:

#### Case A

Initially, the nonyawed case was modeled with a striking velocity of 830 m/s and, for purely economic reasons, the penetrator was modeled using three rings\* (see Figure 4 for comparative gridding sizes).

---

<sup>5</sup>G. H. Jonas and J. A. Zukas, "The Mechanics of Penetration: Analysis and Experiment", Technical Report ARBRL-TR-02137, February 1979.

<sup>6</sup>D. Matuska and J. Osborn, to be published. (AD A068463)

<sup>7</sup>L. D. Bertholf and M. E. Kipp, et. al., "Kinetic Energy Projectile Impact on Multi-Layered Targets: Two Dimensional Stress Wave Calculations", ARBRL-CR-00391, January 1979. (AD B037370L)

\*A ring is a vertical layer. Three rings means three vertical layers per penetrator radius.

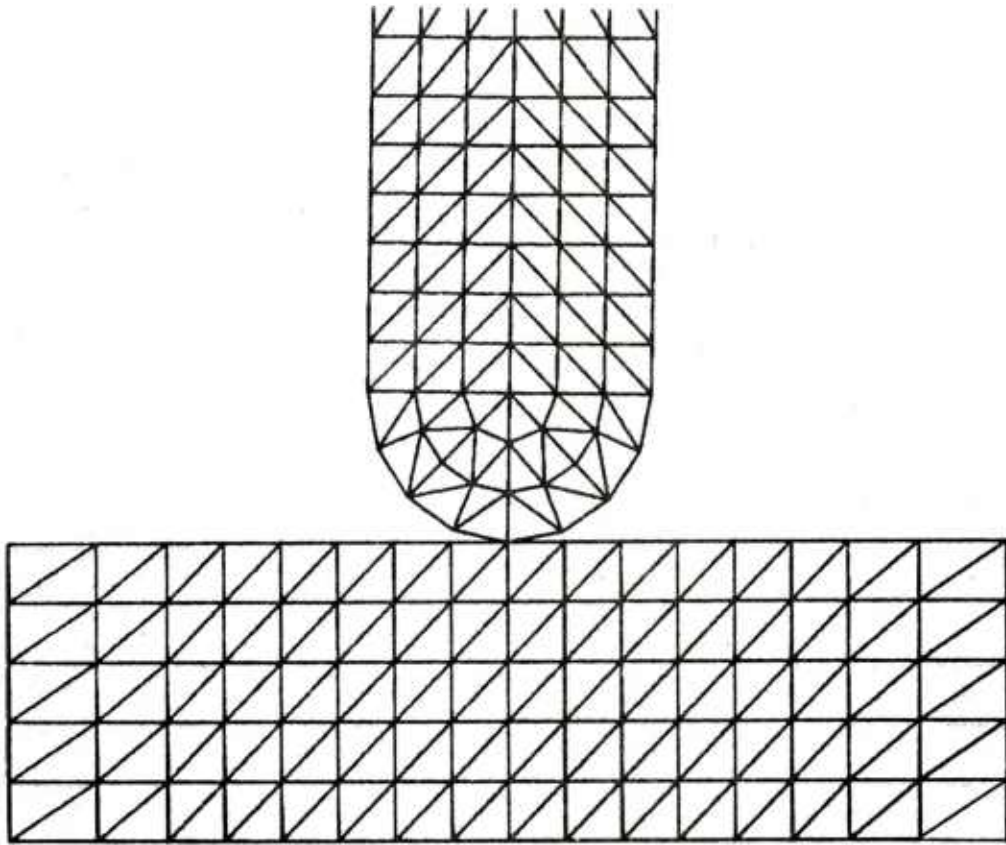


Figure 4a. Comparative Gridding Sizes: 3 Ring Gridding

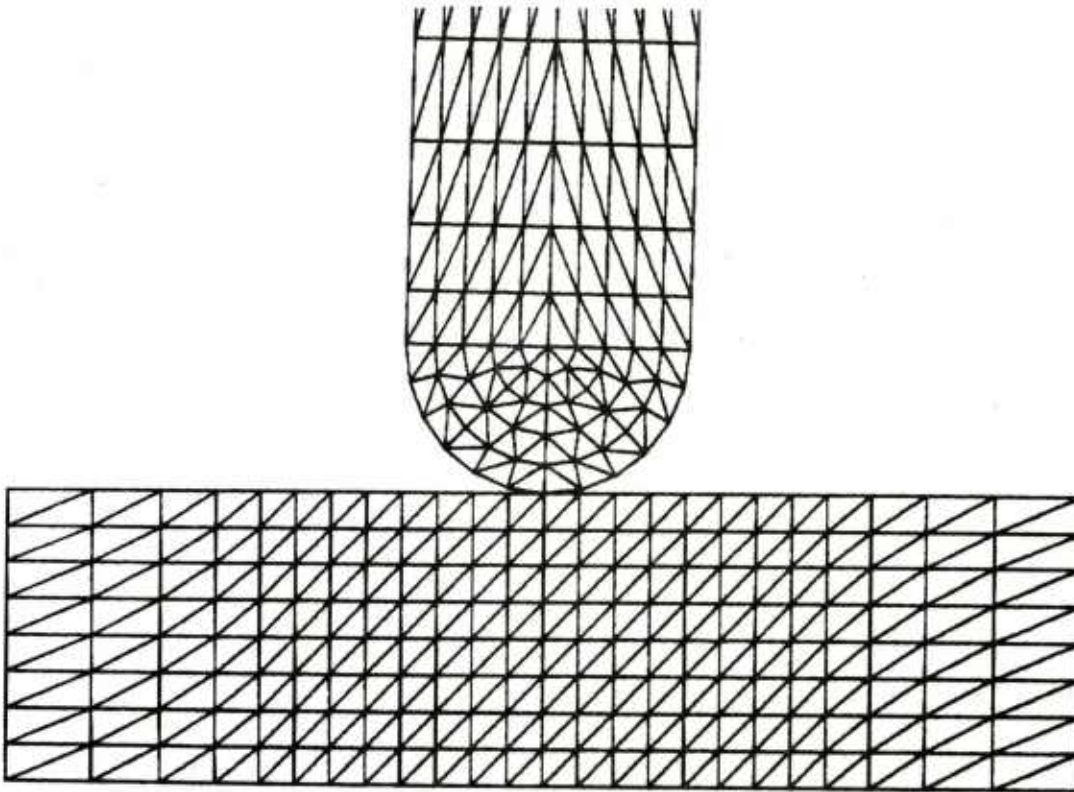


Figure 4b. Comparative Gridding Sizes: 5 Ring Gridding

The material properties shown in Table 2 were used for the penetrator and target. Neither penetrator nor target elements were allowed to fail totally\*. Target elements were allowed to fail in shear and tension\*\* when the equivalent strain\*\*\* reached .35. For the penetrator steel material there were two data points available from Oak Ridge<sup>8</sup>  $\epsilon_f \approx .01$  at strain rate  $\dot{\epsilon} \approx 10^{-4} \text{ s}^{-1}$  and  $\epsilon_f \approx .22$  at  $\dot{\epsilon} \approx 280 \text{ s}^{-1}$ . Therefore .35 seemed reasonable for strain rates  $\approx 10^4$  in RHA. This calculation was stopped at 20  $\mu\text{s}$  (see Figure 5) when the residual velocity of the penetrator was 676 m/s (as compared with experimental results of 674 m/s), the momentum normal to the target was not close to stabilizing and only a slight bulge appeared in the rear of the target instead of a well defined plug. Clearly the coarse gridding resulted in excessively stiff behavior of the target. It was hoped that a finer grid and lower failure criteria would produce better results.

### Case B

Next a finer grid of five rings was attempted with target element failure in shear and tension allowed when the equivalent strain reached 0.2. The calculation stopped at 19.8  $\mu\text{s}$  (see Figure 6) due to an instability in the kinetic energy computation because of gross distortion of a target element.

Realistically, the target elements defining the shear lines surrounding the plug should start to fail gradually from the top of the target to the bottom until the plug is completely "punched out". It was not possible to let the target elements fail gradually however due to the sliding surface treatment (see Appendix A). It had been hoped that the shear lines surrounding the plug would be sufficiently distinct so that the elements defining them would all meet a level of equivalent strain which could be used as the total failure criterion and they could all be failed at once producing a free flying plug. Unfortunately, shear failure was not sufficiently localized to permit unambiguous removal of target elements. Clearly much finer zoning in the target is required.

---

\*Total failure occurs when the equivalent and volumetric strains of an element exceed stipulated values. All stresses including pressure are set to zero for the element. In the cases discussed in this paper, volumetric strain was not considered in stipulated total failure criteria.

\*\*Failure in shear and tension occurs when the equivalent strain of an element exceeds a stipulated value. The element can develop hydrostatic compression but no tensile or shear stresses (i.e., it acts as a liquid).

\*\*\*Equivalent strain is

$$\bar{\epsilon} = \sqrt{2/9 (\epsilon_x - \epsilon_y)^2 + (\epsilon_x - \epsilon_z)^2 + (\epsilon_y - \epsilon_z)^2 + 3/2(\gamma_{xy}^2 + \gamma_{xz}^2 + \gamma_{yz}^2)}$$

where  $\epsilon_x$ ,  $\epsilon_y$ ,  $\epsilon_z$  are normal strains and  $\gamma_{xy}$ ,  $\gamma_{xz}$ ,  $\gamma_{yz}$  are shear strains.

In this version of EPIC-3 the strains are Lagrangian strains.

<sup>8</sup>Dr. E. Bloore, private communication.

Table 2. Material Properties

| Quantity                                 | Projectile             | Target                 |
|--|------------------------|------------------------|
| Density (g/cc)                           | 7.84                   | 7.84                   |
| Elastic Modulus (dynes/cm <sup>2</sup> ) | 2.068x10 <sup>12</sup> | 2.11x10 <sup>12</sup>  |
| Poisson's Ratio                          | 0.28                   | 0.30                   |
| Yield Stress (dynes/cm <sup>2</sup> )    | 1.43x10 <sup>10</sup>  | 8.96x10 <sup>9</sup> * |
| Ultimate Stress (dynes/cm <sup>2</sup> ) | 2.68x10 <sup>10</sup>  | 1.10x10 <sup>10</sup>  |
| Strain at Ultimate Stress                | 0.16                   | 0.22                   |
| Artificial Viscosity Coefficient         |                        |                        |
| Linear Component                         | 0.5                    | 0.5                    |
| Quadratic Component                      | 4.0                    | 4.0                    |

\*This 10mm plate was cut from 38mm plate and softened.

Note: Equation of state data was obtained from "Computation of Hugoniot Equations of State," by Brian J. Kohn, AFWL-TR-69-38, April 1969 (AD 852300).

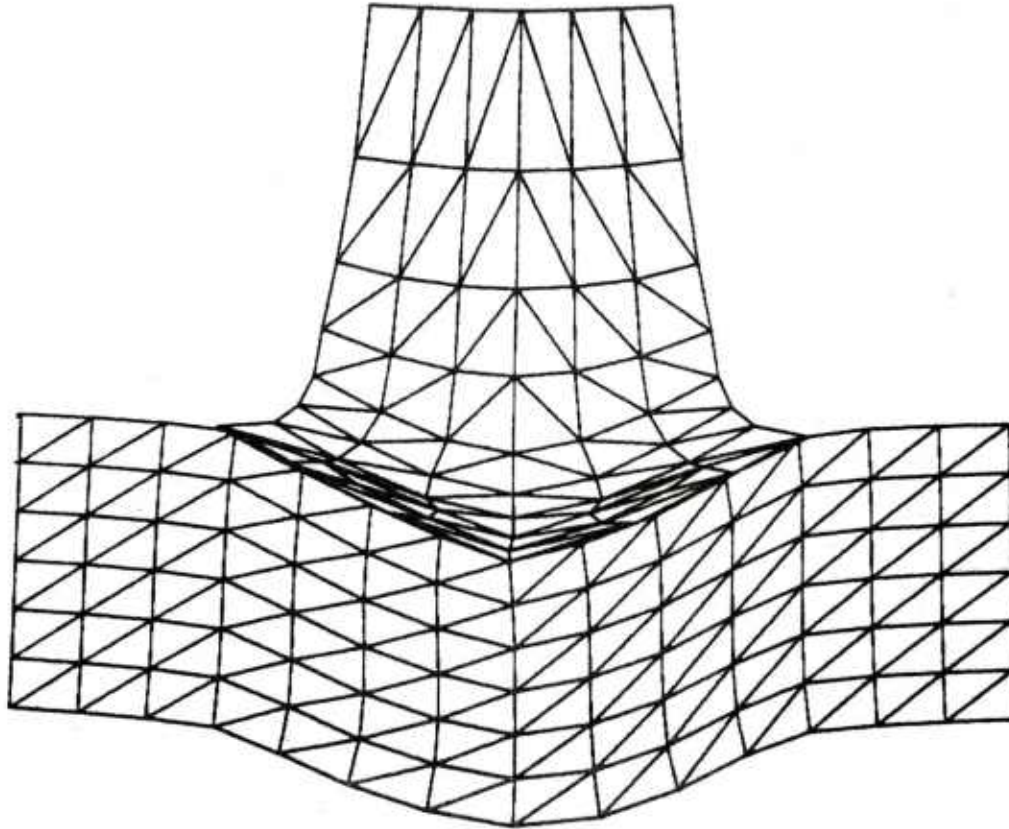
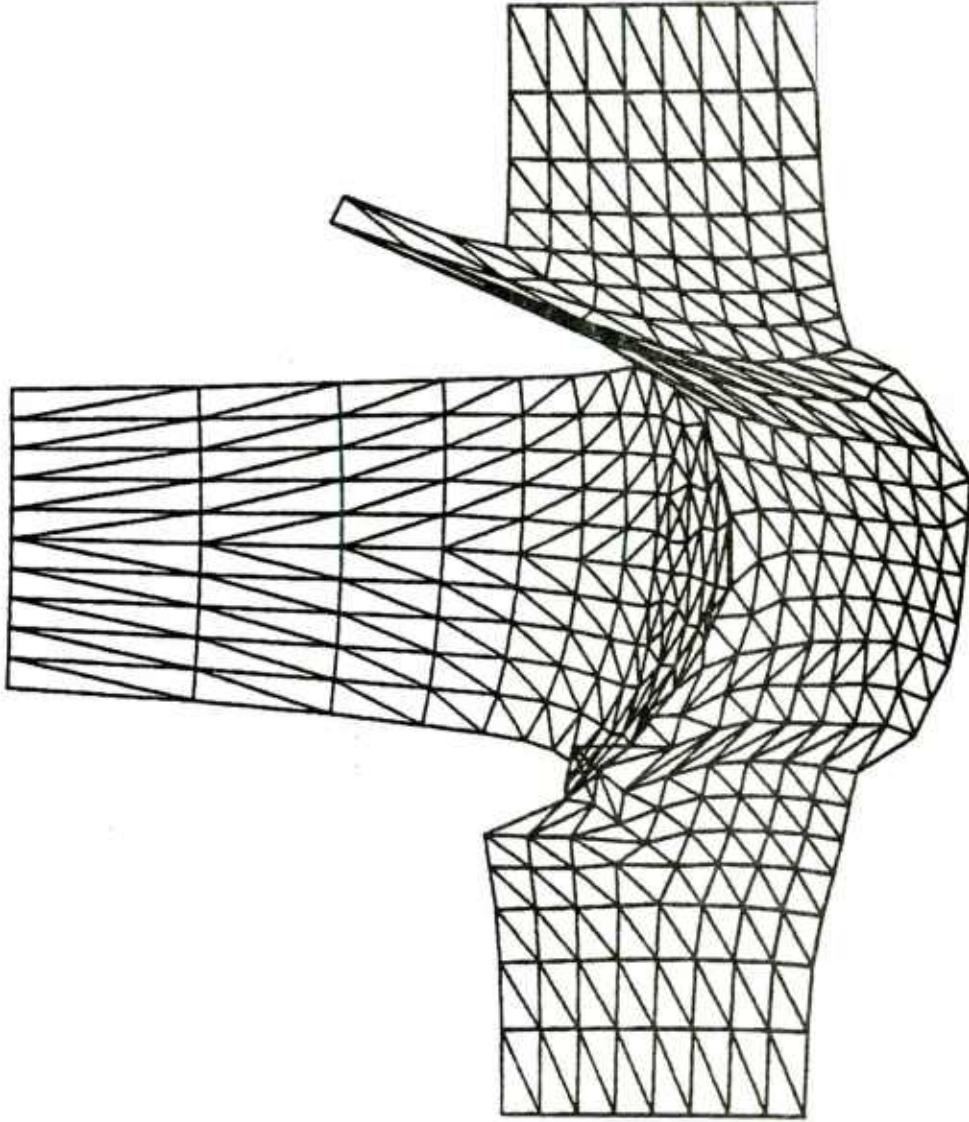


Figure 5. Case A: Nonyawed Penetrator, Coarse Gridding



$t = 20 \mu s$

Figure 6. Case B: Nonyawed Penetrator, Fine Gridding

12 FEB 79

Figure 6 shows the plug in an incipient stage. However, the residual velocity of the penetrator (722 m/s) indicates that the plug is not forming quickly enough for the residual velocity of the penetrator to approximate the experimental value of 674 m/s after it has sent the plug on its way at 676 m/s. There are two other details to be noted in this cross-sectional deformation plot. There was less than  $1^\circ$  total yaw so the results would not be expected to be truly symmetric. However, there is a greater lack of symmetry in the results due to a lack of geometrical symmetry of elements about the center of the target (considered to be coincident with the tip of the projectile, see Figure 5). This is the way the geometry generation in EPIC-3 handles target elements. There is a cross-over between the penetrator and target on the left side of the plug; the slave node spacing has surpassed the master node spacing with the result that consecutive slave nodes affect master surfaces which are not consecutive. There is a master surface between them which is not affected. This has been alleviated in the revised version of the code where infringement of master nodes on slave surfaces is also checked.

#### Case C

The yawed case was started when the nonyawed case had looked promising so it was allowed to continue until it halted at 20.7  $\mu$ s (see Figure 7) when instabilities in energy computations occurred. The same material properties were used for the yawed case; the striking velocity was 840 m/s. The residual velocity was 727 m/s when the calculation stopped but again, the plug has been slow in forming. It is interesting to note that considerable yaw seems to have had little effect on residual velocity up to 20  $\mu$ s. Compare this with the nonyawed case which had a striking velocity of 830 m/s and a residual velocity of 722 m/s at 19.8  $\mu$ s.

#### Case D

Dr. Gordon Johnson, the author of EPIC-3, suggested that since the code had indicated the location of the shear lines defining the plug the problem could be initially set up taking this into account. Normally, for a monolithic target, the target elements are all considered to be one material. However, for this case, the target elements were to be assigned separate but identical materials, one for those elements which belonged to the plug, a second for those which occurred around the circumference of the plug (the shear lines) and a third, the remainder of the target. When the plug had sufficiently formed, the elements with the second material could be artificially failed and the plug permitted to fly freely. The code was changed to accomplish this and three ring gridding was used for this iteration. Note that this approach, though artificial, is the analog of current practice with finite difference impact codes where problems are initially run to determine the positions where plugging is expected to occur and then the problem is rerun with slide lines introduced at those positions so that the anticipated plug can form along predetermined lines.

TIME = .00002070

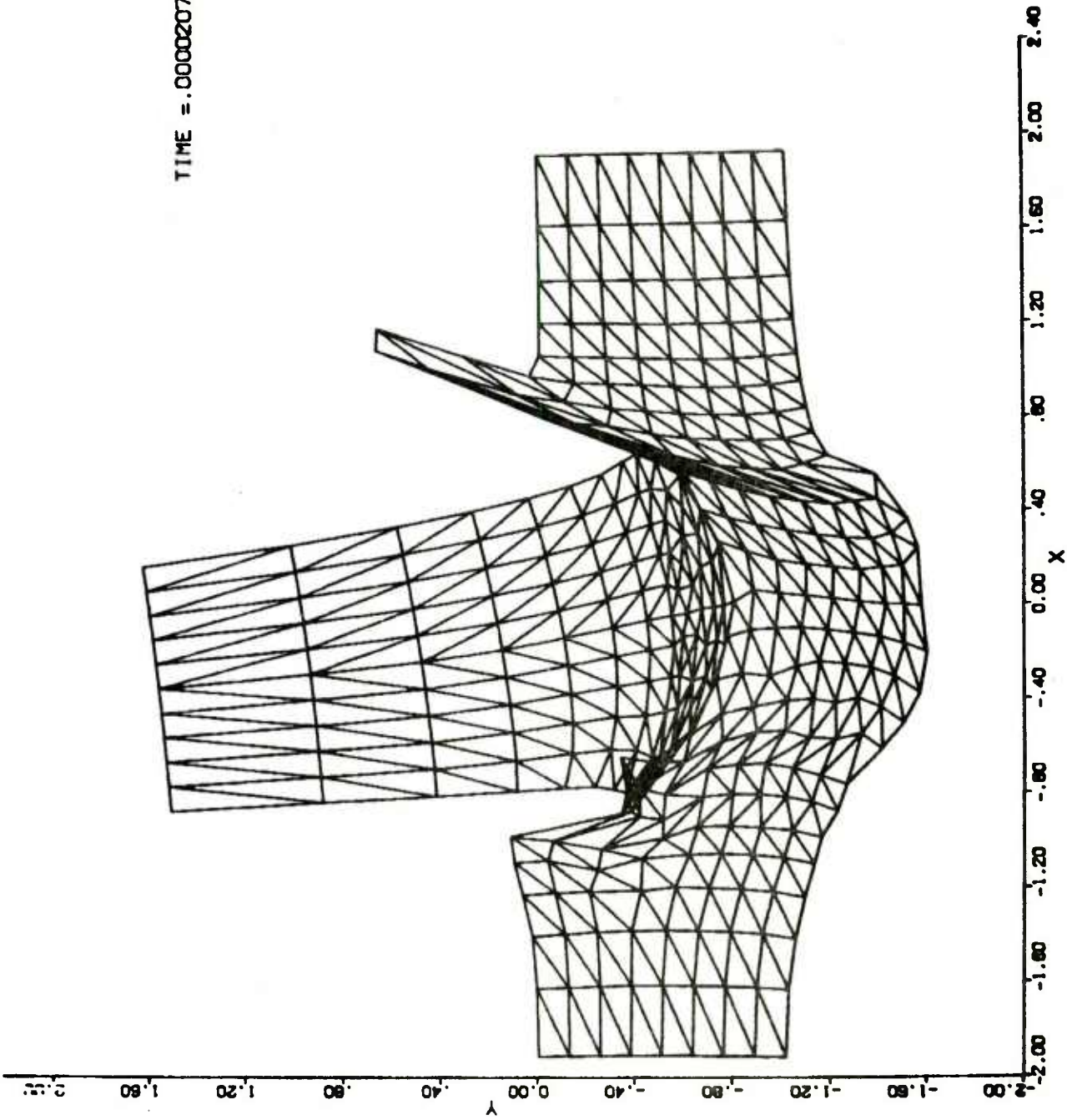
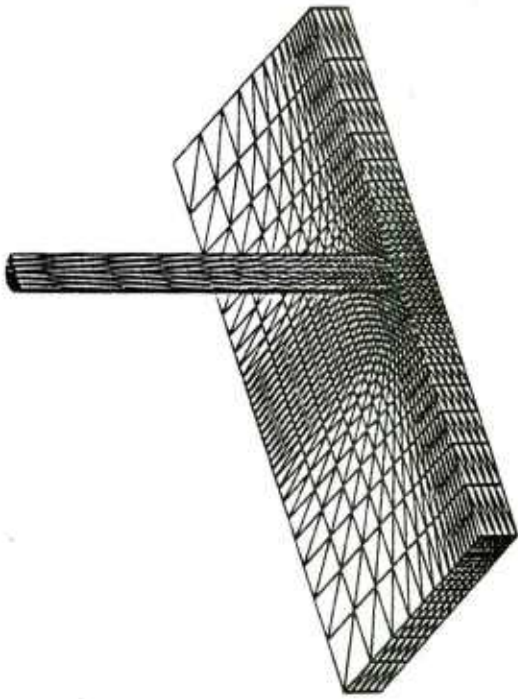


Figure 7. Case C: Yawed Penetrator, Fine Gridding

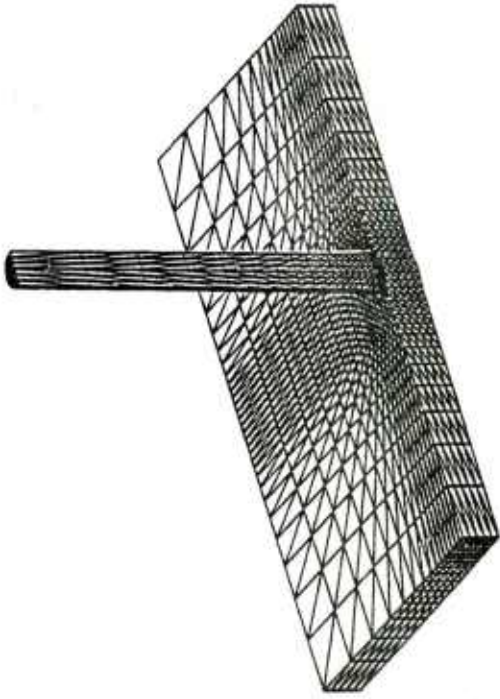
The projectile elements were allowed to fail in shear and tension when the equivalent strain reached .2 and fail totally when the equivalent strain reached 1. This was done in an attempt to model the erosion of the nose of the penetrator and also alleviate the problem of unrealistic severe distortions in the target surface elements due to a nondeforming projectile. The target elements, regardless of material designation, were allowed to fail in shear and tension when the equivalent strain reached .25 but they were not allowed to fail totally. Isometric deformation plots showing the progress of the calculation are shown in Figure 8.

At 30  $\mu\text{s}$  a realistically-shaped plug had formed, the coarse grid and poorly formed shear lines precluding a distinct plug as expected. The shape of the plug and the residual velocity of the penetrator at this time (675 m/s) warranted releasing the plug. The elements around the circumference of the plug were artificially failed as planned. Cross-sectional and isometric plots of the resulting situation are shown in Figures 9a and 9b.

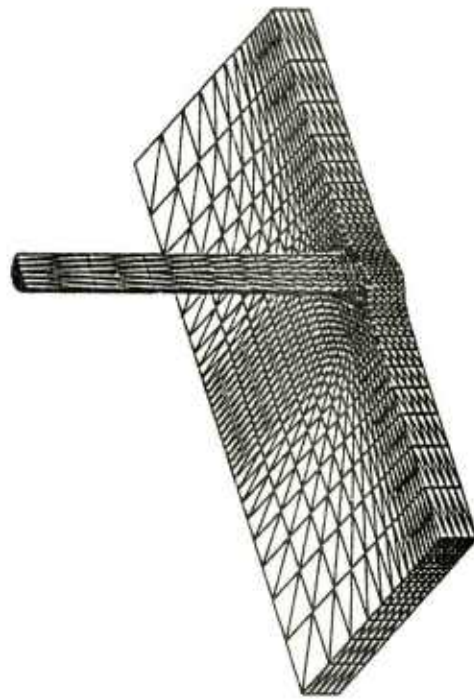
The calculation stopped at 50  $\mu\text{s}$  when plug elements became severely deformed. The residual velocity of the penetrator at 50  $\mu\text{s}$  was 655 m/s as compared with 674 m/s experimentally. However the residual velocity of the plug, 328 m/s (up from 278 m/s when first released) and the V shape of the plug (see Figures 10a and 10b for cross-sectional deformation plots at 25  $\mu\text{s}$  and 45  $\mu\text{s}$ ) were due to the relatively low value of equivalent strain which had been used (.25) for target element failure in shear and tension. Unfortunately this low criterion had also been achieved by most of the elements in the plug so the plug acted essentially as a fluid, able to develop hydrostatic pressure but certainly not able to act as a rigid-bodied plug. Further pressure from the penetrator only caused the plug to flow up around the penetrator rather than be propelled ahead. Note that at 45  $\mu\text{s}$  there is an overlap of plug and other target material. No sliding surface relationship existed between these surfaces so they are unaware of each other's existence.



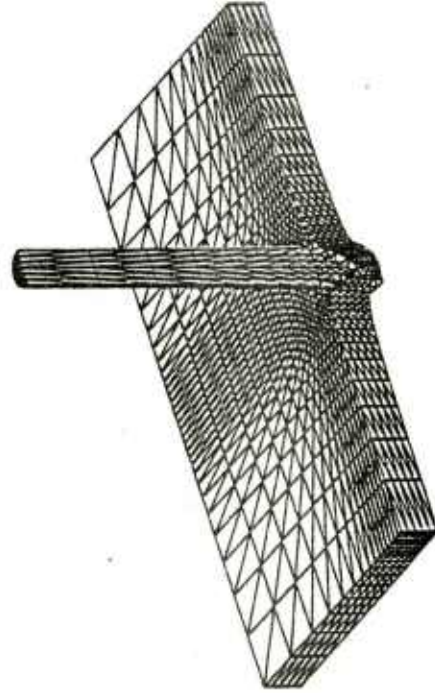
$t = 0 \mu s$



$t = 5 \mu s$



$t = 15 \mu s$

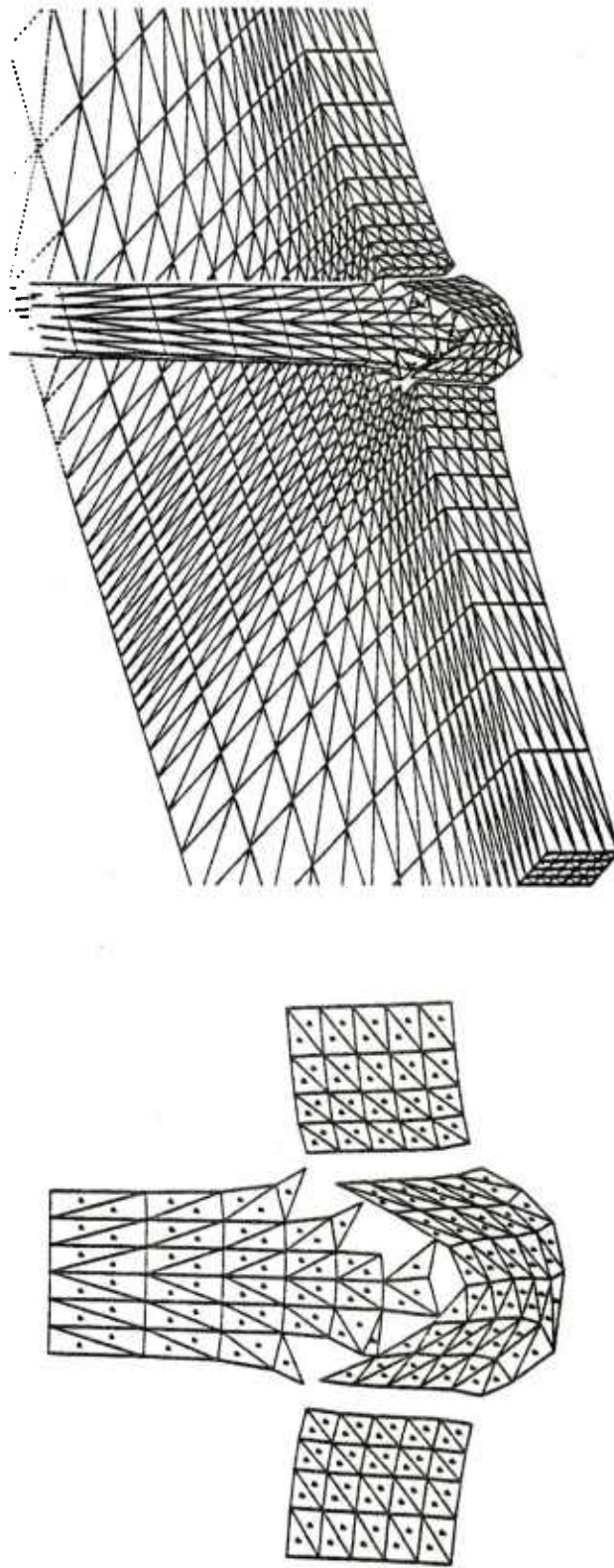


$t = 30 \mu s$

12 FEB 79

Figure 8. Case D: Isometric Deformation Plots of Nonyawed Penetrator at Four Time Steps

# RELEASE OF PLUG



$t = 30.1 \mu s$

Figure 9a. Case D: Cross-Sectional Deformation Plot of Release of Plug

Figure 9b. Case D: Isometric Deformation Plot of Release of Plug

12 FEB 79

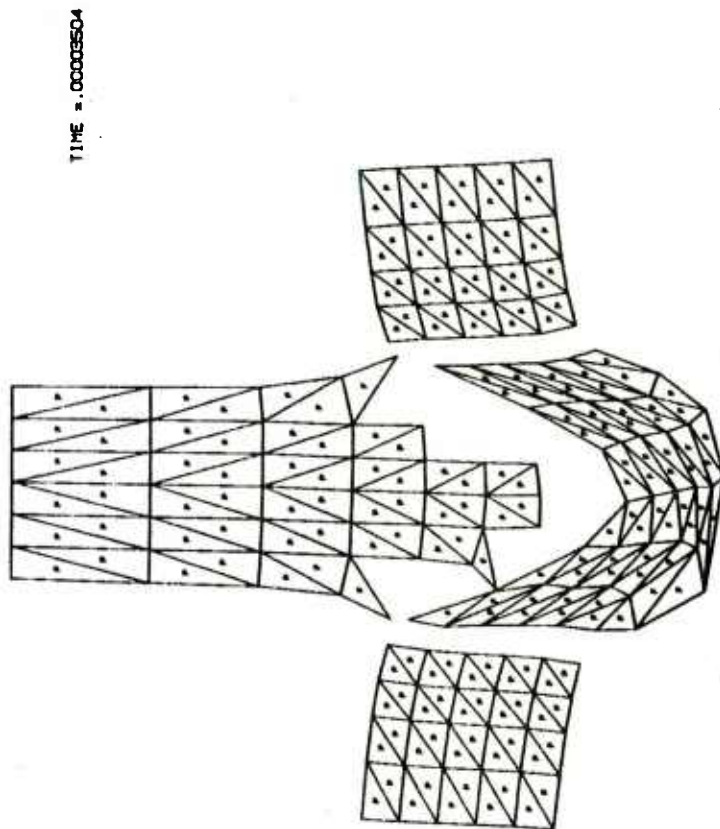


Figure 10a. Case D: Cross-Sectional Deformation Plot at 25  $\mu$ s

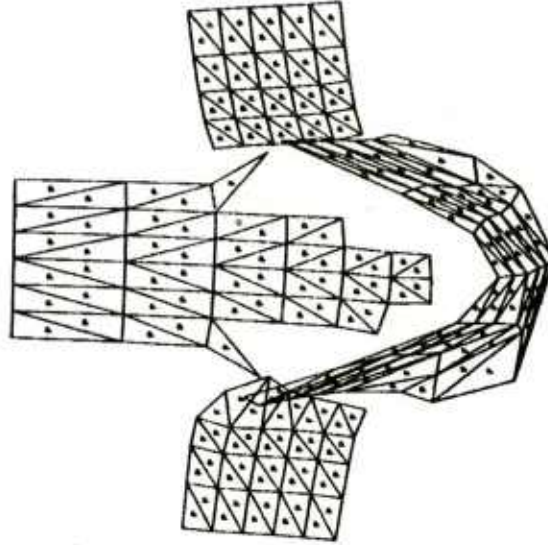


Figure 10b. Case D: Cross-Sectional Deformation Plot at 45  $\mu$ s

The predicted length of the residual penetrator was 8.3cm as compared with the experimental value of 8.16cm. The artificially produced plug had a mass of 11.6 g as compared with 12.1 g obtained experimentally.

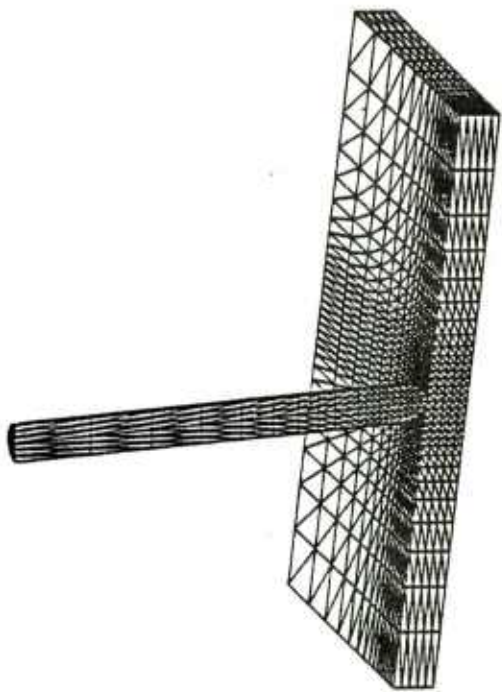
#### Case E

In the yawed case, as in the nonyawed case, .2 and .25 were used as the values of equivalent strain for which failure in shear and tension would occur in the projectile and target respectively. The target elements were not allowed to fail totally. The projectile elements were allowed to fail totally when the equivalent strain reached 3 versus 1 for the nonyawed case. Isometric deformation plots showing the progress of the calculations are seen in Figure 11. A rather jagged-looking plug appeared by 15  $\mu$ s resulting largely from the higher strain required for total failure\*. The coarser grid (three versus five rings) also seemed more critical in the yawed case. Based strictly on the jagged appearance of the deformation, the decision was made to reduce the criterion for total failure in the projectile elements to 2 after 15  $\mu$ s. At 35  $\mu$ s when the penetrator residual velocity was 648 m/s the plug was artificially released and is shown at 45  $\mu$ s in Figure 13. The momentum had not stabilized and the plug was very jagged-looking, unlike that seen in the radiographs. Shortly after 45  $\mu$ s the calculation stopped when the kinetic energy exceeded the original by 10% as one of the plug elements had become severely deformed. At 45  $\mu$ s the penetrator residual velocity was 631.4 m/s, the plug velocity, 372 m/s as compared with 550 m/s and 663 m/s obtained experimentally for the residual penetrator and plug respectively.

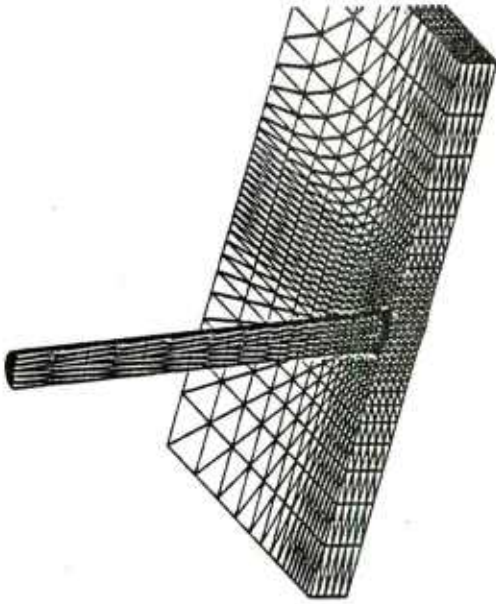
The low velocity and V-shape of the plug were due to the fluid condition of the plug as described in the nonyawed case. The calculation stopped just as the left edge of the target was starting to affect the side of the penetrator. (See the cross-sectional deformation plots in Figure 14.) It had been hoped that the large bend further along the rod (shown in the radiographs) would be crudely simulated in the calculation.

---

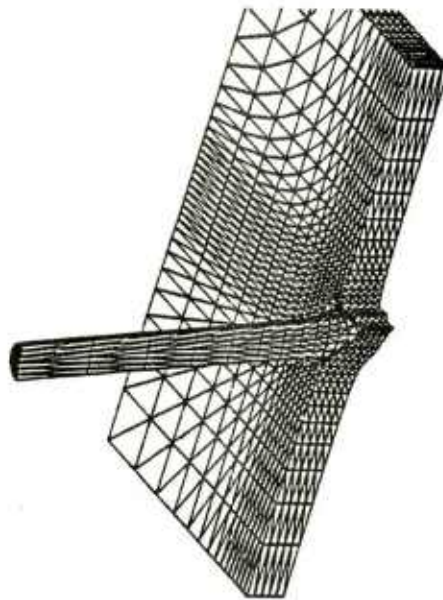
\*In trying to determine the cause of such jaggedness, the same failure criteria were subsequently used for the nonyawed case with the same jagged looking results (see Figure 12) so the higher strain required for total failure was the cause but it is not known why it had this effect.



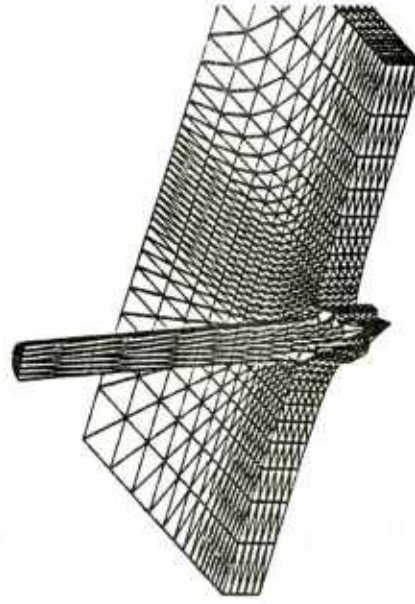
$t = 0 \mu s$



$t = 5 \mu s$



$t = 25 \mu s$



$t = 35 \mu s$

Figure 11. Case E: Isometric Deformation Plot of Yawed Penetrator at Four Time Steps

12 FEB 79

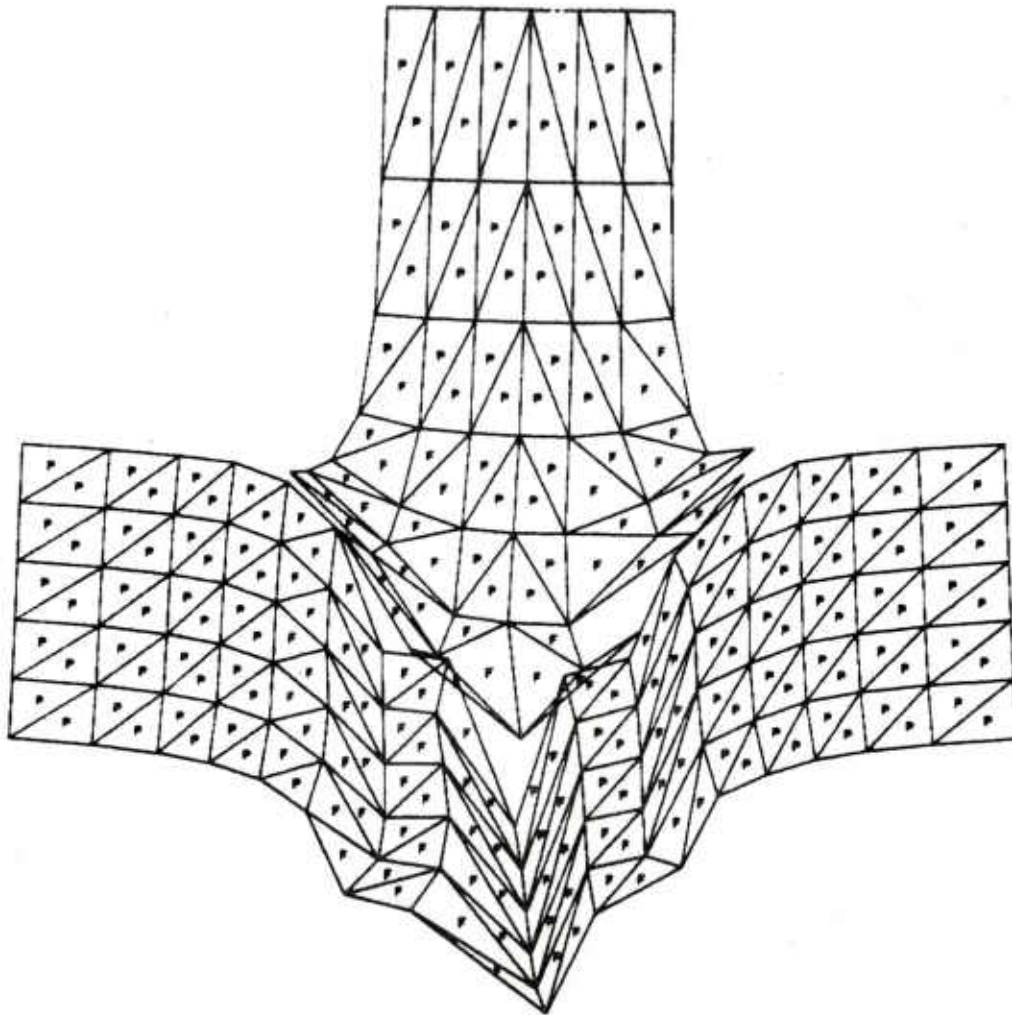


Figure 12. Cross-Sectional Deformation Plot of Nonyawed Penetrator at  
30  $\mu$ s With Total Failure occurring When the  
equivalent strain = 3

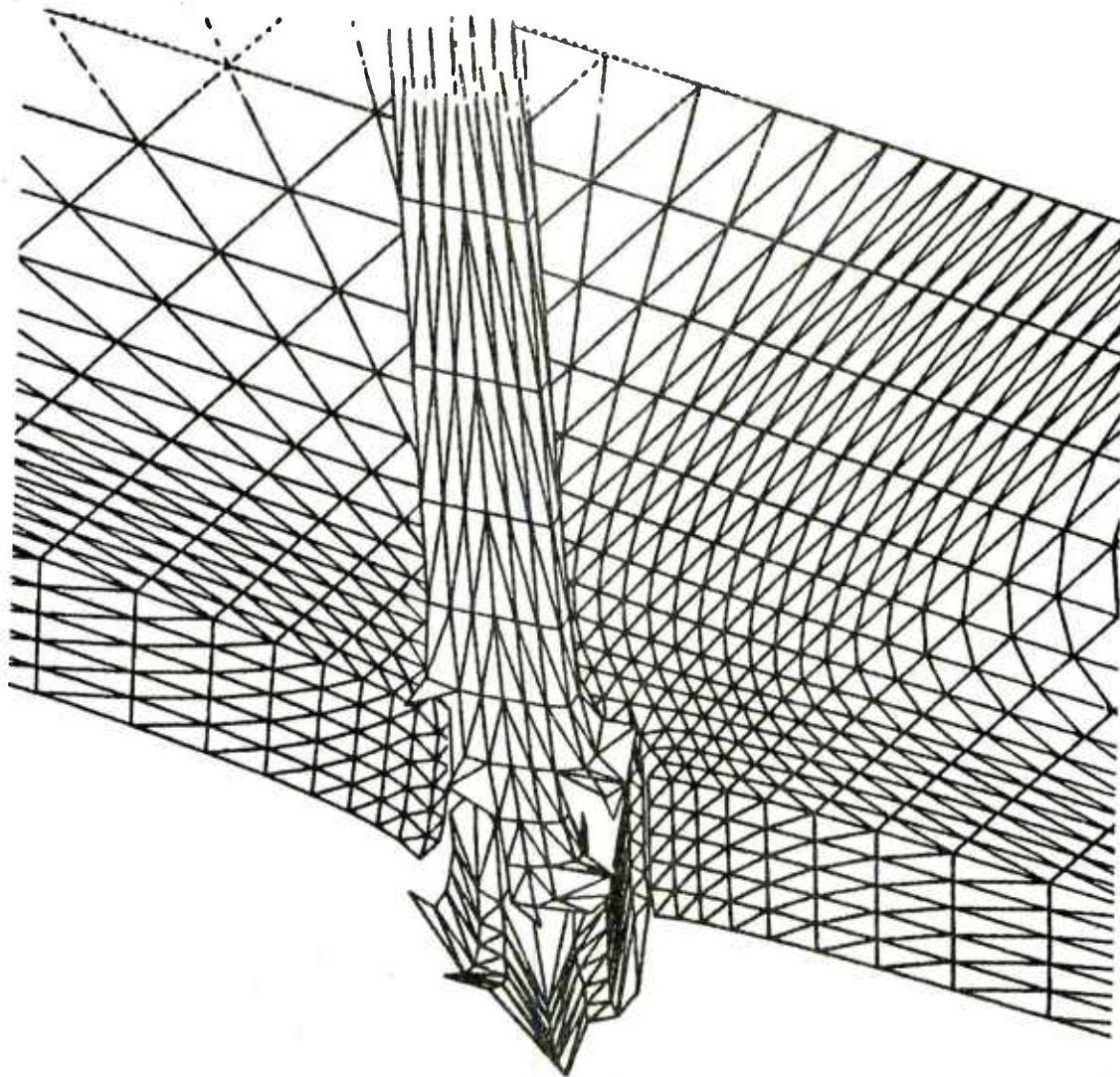


Figure 13. Case E: Isometric Deformation Plot of Yawed Penetrator at 45  $\mu$ s After Release of the Plug

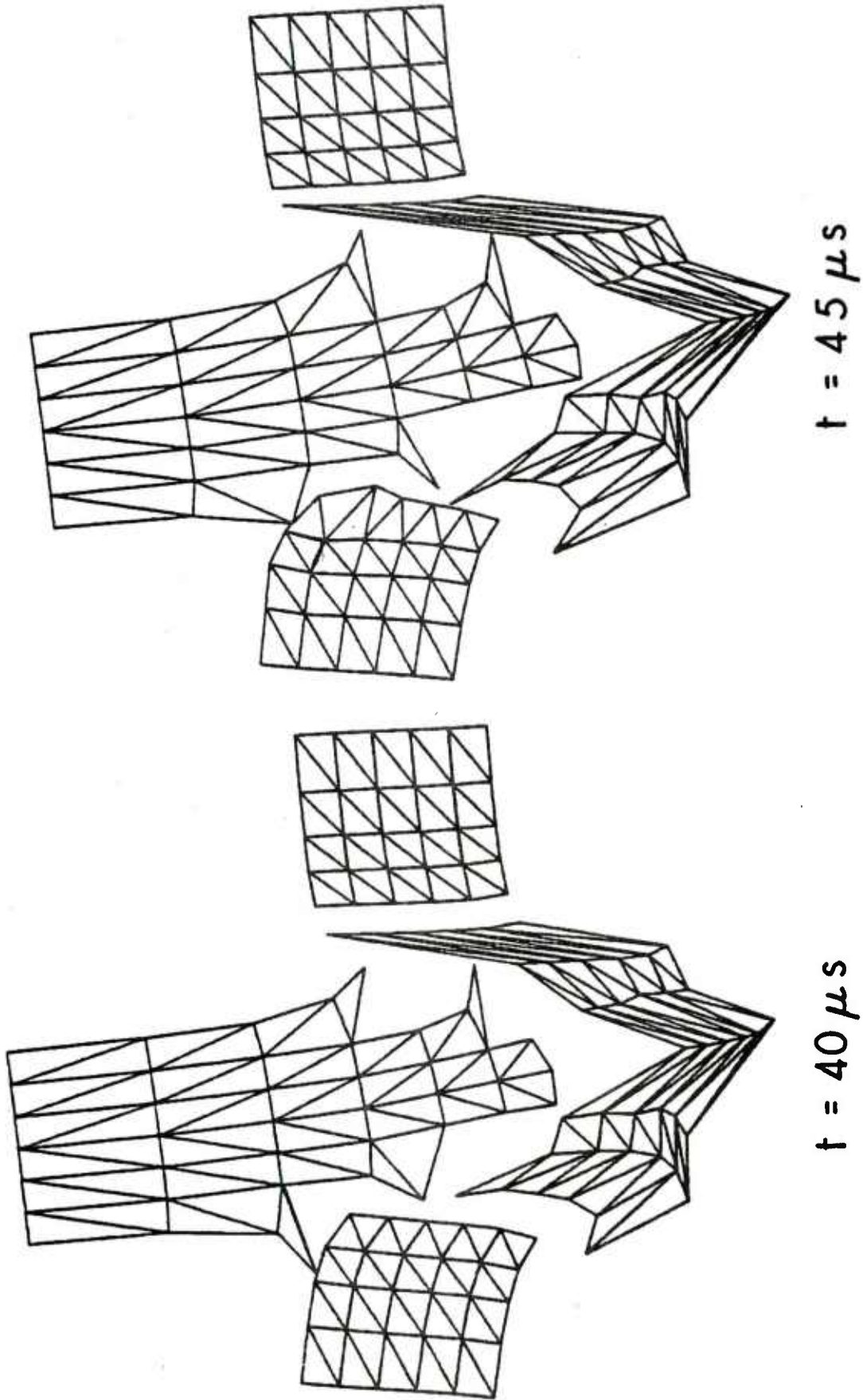


Figure 14. Case E: Cross-Sectional Deformation Plots of Yawed Penetrator at 40 and 45  $\mu s$  12 FEB 79

Experimentally, the far end of the penetrator had finally broken off, probably due to this second impact. This should account for most of the disparity in the residual rod length between the experimental results (5.94cm) and the calculated prediction 7.67cm.

This is an excellent example of an impact situation in which the remaining target material can not be simply discarded if a valid simulation is to be produced. The results were not as good in the yawed case as in the nonyawed case. The coarser gridding and the higher equivalent strain required for total failure in the projectile appeared to have a greater effect on the results. Also, the calculation could not go far enough to obtain the effect of the target edge on the yawed rod, the probable primary factor in the difference between yawed and nonyawed impact residual rod orientation. Experimentally, the diameter of the plug was considerably larger in the yawed case (1.7cm) as compared with the nonyawed case (1.49cm) and the diameter of the projectile (1.02cm). Therefore, the predetermined boundary of the plug based on elements specified a radius (slightly larger than the radius of the projectile) from the center was a cruder model in the yawed case, so the artificial plug with a mass of 11.6 g was a poorer approximation to the plug mass obtained experimentally (13.21 g) as seen in the radiographs.

Table 3 gives a summary of experimental vs simulation results for the nonyawed (Case D) and yawed (Case E) impacts respectively.

#### IV. NUMERICAL SIMULATION USING REVISED EPIC-3

An improved version of EPIC-3<sup>2</sup> was received during the course of these calculations. The revised code, although similar to the earlier version<sup>1</sup>, contains many extensions and improvements, among them:

- a. an incremental elastic-plastic formulation. This permits correct simulation of material unloading as opposed to the total elastic-incremental plastic formulation of Reference 1.
- b. an improved treatment of internal energy computations so that total energy is better conserved.

The revised version of EPIC-3 was used to compute the impact of a 27.1 gram S7 steel rod, L/D of 10 into a 12.5mm single RHA target at 40° yaw. The striking velocity was 927 m/s. Experimental data for this situation was obtained from Mr. C. Grabarek. Material properties for the computation are given in Table 4 and computational results shown in Figure 15. A true stress-true strain formulation is used in the revised EPIC-3 whereas a Lagrangian strain measure had been employed in the original version. The penetrator elements were allowed to fail

Table 3. Experimental vs. Simulation Results

|                     | Nonyawed Case<br>(less than 1° total yaw) |                    | Yawed Case<br>(6.86° total yaw) |                    |
|---------------------|---|--------------------|---------------------------------|--------------------|
|                     | Experiment                                | Calculation        | Experiment                      | Calculation        |
| Striking Velocity   | 834 m/s                                   | 830 m/s            | 841 m/s                         | 840 m/s            |
| Total Yaw           | .97°                                      | .97°               | 6.86°                           | 6.86°              |
| Residual Velocity   | 674 m/s                                   | 655 m/s @<br>50 μs | 550 m/s                         | 631 m/s @<br>45 μs |
| Residual Rod Length | 8.16 cm                                   | 8.3 cm             | 5.94 cm                         | 7.67 cm            |
| Plug Velocity       | 676 m/s                                   | 328 m/s*           | 663 m/s                         | 372 m/s*           |
| Plug Mass           | 12.17 g                                   | 11.6 g             | 13.21 g                         | 11.6 g             |

\*The liquid condition of the plug effectively nullifies these results.

Table 4. Material Properties for 4° Yaw Computation

| Quantity                                 | Projectile            | Target                |
|--|-----------------------|-----------------------|
| Density (g/cc)                           | 7.84                  | 7.84                  |
| Elastic Modulus (dynes/cm <sup>2</sup> ) | 2.07x10 <sup>12</sup> | 2.07x10 <sup>12</sup> |
| Poisson's Ratio                          | 0.28                  | 0.30                  |
| Yield Stress (dynes/cm <sup>2</sup> )    | 1.86x10 <sup>10</sup> | 1.1x10 <sup>10</sup>  |
| Ultimate Stress (dynes/cm <sup>2</sup> ) | 2.24x10 <sup>10</sup> | 1.52x10 <sup>10</sup> |
| Strain at Ultimate Stress                | 0.10                  | 0.16                  |
| Artificial Viscosity Coefficient         |                       |                       |
| Linear Component                         | 0.2                   | 0.2                   |
| Quadratic Component                      | 4.0                   | 4.0                   |

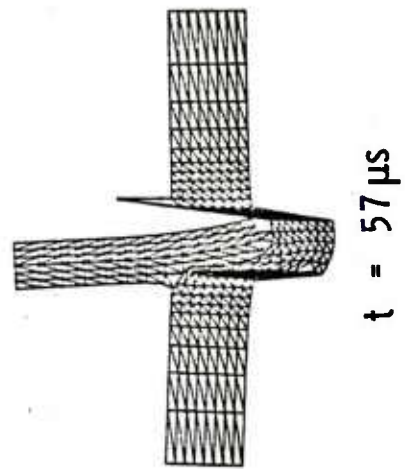
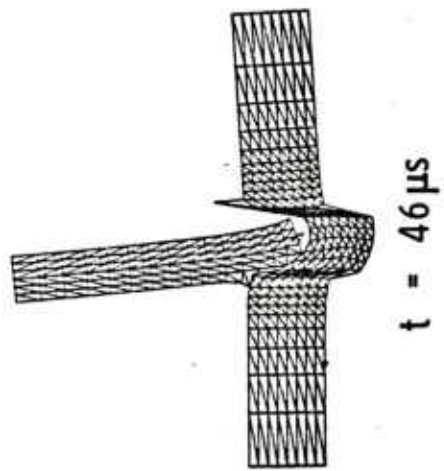
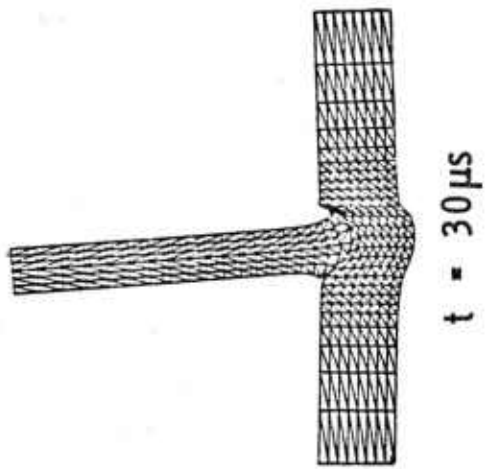
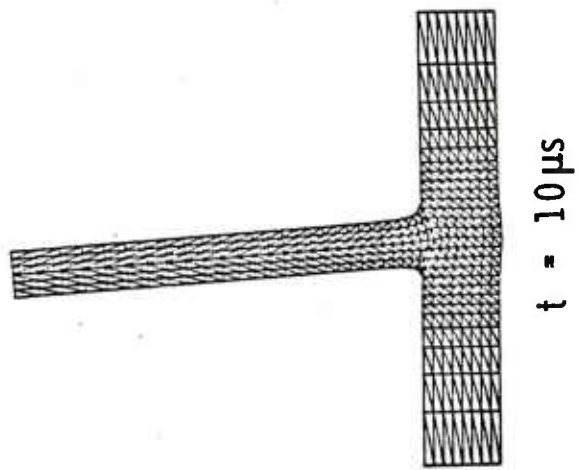


Figure 15. Cross-Sectional Plots of  $4^\circ$  Yaw Case Using Revised EPIC-3

in shear and tension when the equivalent strain reached .25 and totally when the equivalent strain reached 1.5. The target elements were allowed to fail in shear and tension when the equivalent strain reached .32; they were not allowed to fail totally. It can be seen from Figure 15 that the shear lines, even for this coarsely gridded case, are much more distinct than in previous calculations. The residual velocity at 57  $\mu$ s of 581 m/s compares favorably with the experimental value of 556 m/s. The velocities for the nodes associated only with failed elements were excluded from the residual velocity determination which is more accurate than the results for the previous calculations which included the velocities of nodes which were no longer a part of the residual penetrator. There is also excellent correlation for the residual penetrator mass (12.97 g vs. 12 g obtained experimentally), the nodal mass of free flying nodes being excluded. However, as in the previous results, plug elements have also failed, rendering it in effect a fluid.

## V. CONCLUSIONS

From the foregoing, we may draw several conclusions regarding requirements for adequate simulation of plugging problems.

a. Very fine spatial resolution is required in attempting to model the plugging involved in ballistic impact situations. Even though the results shown in Figure 15 have visual appeal, the fluid state of the plug indicates the need for a fine mesh in order to concentrate the activity. Fine resolution will increase considerably the cost of three-dimensional computations. For example, a computation with 15,372 elements from 0-20  $\mu$ s required 2700 CPU seconds whereas the same calculation with 38,184 elements required 14,000 CPU seconds.

b. If feasible, investigation into plugging phenomena ought to be undertaken initially with two-dimensional impact codes in an attempt to model the plugging involved in normal impact situations. This would provide great reductions in the time, cost, and complexity involved. Once some success has been attained with this relatively simple plugging situation, then the same techniques may be applied using three-dimensional impact codes to enable further refinement and verification.

c. Investigation must be conducted as to which failure criteria should best handle plugging failure. Since plugging is a complex mode of failure, probably due to different mechanisms depending on the materials and strain rates involved, various types of plugging failure must be studied. An effective plastic strain criterion by itself may not be adequate to handle any or all of these.

For typical ballistic impact situations involving high strain rates and RHA targets, it is thought that a plastic shear instability occurs at the projectile periphery resulting in adiabatic shear and subsequently

plugging failure. The work of plastic deformation is converted almost entirely into heat which, because of high deformation rates, is unable to diffuse significantly away from this narrow plastic zone. The temperature in the zone rises and thermally softens the local material, encouraging and concentrating additional local plastic flow. Hence, failure criteria to model these situations ought to include treatment of thermal softening. Another possibility is the incorporation of a failure model based on shear strains and shear strain rates. Experimental work for RHA along these lines is being conducted by Dr. G. Moss<sup>9</sup> of BRL and analytical models for shear nucleation and growth suitable for incorporation in two- and three-dimensional computer codes are under development at Stanford Research Institute<sup>10</sup>.

d. The earlier version of EPIC-3<sup>1</sup> lacks many of the necessary features needed for the study of highly localized deformations. Its use is not recommended for these or other problems in view of the availability of improved versions of EPIC-3.

#### ACKNOWLEDGEMENT

The author wishes to thank Dr. Jonas Zukas for suggesting the problem and method of solution.

---

<sup>9</sup>Dr. G. Moss, private communication.

<sup>10</sup>Dr. D. Curran, private communication.

APPENDIX A  
Sliding Surface Treatment

In the current version of EPIC-3 sliding surfaces are used to handle the interface between different surfaces (e.g., target and penetrator). Usually the master surface is assigned to the target and the slave surface is assigned to the penetrator. If a slave node penetrates the master surface it is moved onto the master plane, normal to its surface and its lost momentum is transferred to the nodes defining that master plane. This necessitates the master surface remaining intact where there is any possibility of a slave node interfering. Otherwise, a slave node will not be aware of any other surfaces so will not be restrained in any way.

When a thin target suffers severe deformation (see Figure A1) and the penetrator momentum normal to the target has stabilized, it is realistic to fail all of the target material below the projectile at once, assuming there is no concern for possible ballistic effects due to this failed material.

However, realistically, in the case of a thick target, portions of the top layer will fail much sooner than portions of the bottom layers. There is at present a contract with Honeywell to change the sliding surface treatment to allow a master element to fail and transfer its master status to the element directly below it. It is hoped that this improvement will enable accurate simulation of deep penetration problems.

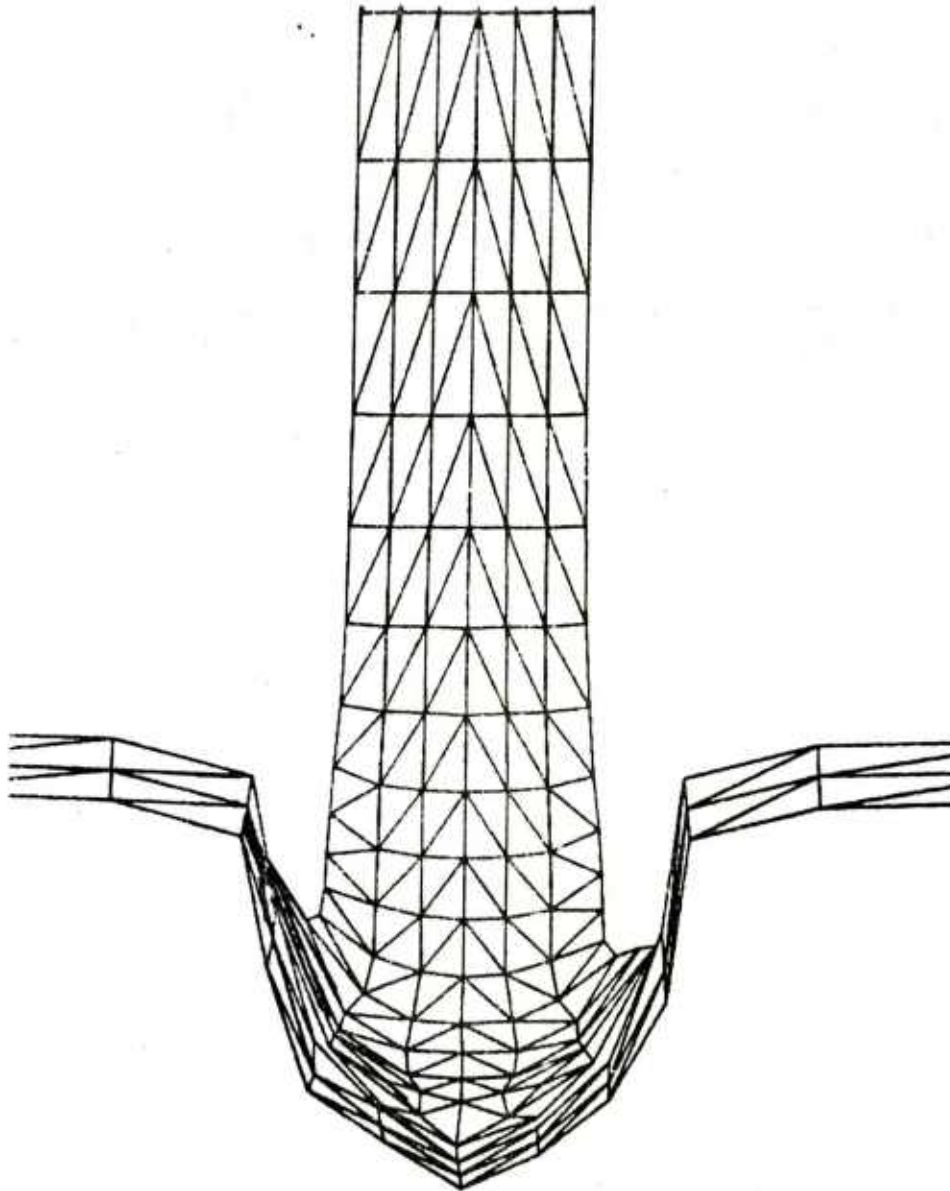


Figure A1. Severe Deformation of Thin Target

APPENDIX B  
Definitions

1.  $V_S, V_R$  Test - the firing of a number of nominally identical penetrators into as many nominally identical targets with all controlled phenomena except striking velocity being nominally invariant (i.e. a fixed "projectile-target situation"); penetrator striking and residual velocities from each shot are measured and a collection of data points ( $V_S, V_R$ ) is thereby generated.

The primary purpose of conducting a  $V_S, V_R$  test is to analyze the dependence of residual velocity on striking velocity (including limit velocity determination) for a specified projectile-target situation. The radiographic coverage needed for velocity measurement provides relatively easy access to further penetration mechanics analysis: frequent additional objectives in  $V_S, V_R$  testing involve, for instance, study of the dependence on striking velocity of various residual effects (e.g., residual penetrator mass; the shape, mass, and velocity of a plug or of other fragment debris).

2. Limit Velocity ( $V_\ell$ ) - value determined from a set of  $V_S, V_R$  data (as generated in a  $V_S, V_R$  test) using the computational algorithm described in BRLR 1852 (AD A021389);  $V_\ell$  is one of a triple of values ( $a, p, V_\ell$ ) which minimizes the root mean square error when the form

$$V_R = \begin{cases} 0, & 0 \leq V_S \leq V_\ell \\ a(V_S^p - V_\ell^p)^{1/p}, & V_S > V_\ell \end{cases} \quad \text{is applied to the given } V_S, V_R$$

data set.

Note: the idealized physical notion abstracted to suggest the above form is that of an absolutely invariant projectile-target situation for which each striking velocity can yield one and only one residual velocity (and the  $V_\ell = \max \{V_S: V_R = 0\} = \inf \{V_S: V_R > 0\}$ ).

3. Incidence Angle (or Obliquity) ( $\theta$ ) - angle between the penetrator line of fire (path of the center of gravity) and the normal to the target plane.
4. Spacing between plates - orthogonal distance between plates.
5. Plug - a major fragment which may be punched out from the target, usually at striking velocities near the limit velocity. A plug

These definitions are taken from:

Lambert, J. P. and Ringers, B. E., "Standardization of Terminal Ballistics Testing, Data Storage and Retrieval", Technical Report ARBRL-TR-02066, May 1978. (AD A056366)

is of roughly cylindrical shape having diameter at least as large as that of the penetrator and height (or length) no greater than the target plate thickness; front and rear ends tend to be convex and concave respectively and the lateral surface shows strong indication of shear.

6. Perforation - passage of a penetrator completely through a target. In terms of velocity, we say there is perforation if and only if  $V_r > 0$ .
7. Striking Velocity ( $V_s$ ) - velocity (really, speed) of penetrator at impact; determined from the position, time history of before-target radiographic images.

The following geometric setting will be used in describing items 29 and 30 (Figures B1 and B2). Consider a coordinate system in which the origin is on the line of fire at a point midway through the target plate, the z-axis coincides with the line of fire, and the x and y axes are respectively horizontal and vertical with respect to the test set-up. (In the context of usual experimental procedure, this means that the x-axis is parallel to and midway between the front and rear target surfaces and that the y-axis makes with these surfaces an angle equal to the obliquity.)

Note: Wherever used, the term "residual penetrator" will refer to the major (largest) post-perforation penetrator remnant, while "residual length" will refer to the length, as measured along the longitudinal axis, of the residual penetrator.

8. Cone Angle ( $\lambda$ ) and Phase Angle ( $\phi$ ) - these are behind-target characteristics descriptive of the trajectory of the residual penetrator (see Figure B1). Let  $P = (x_o, y_o, z_o)$  be the center of the gravity of the residual penetrator at some point behind the target. The Cone Angle is the acute angle between the line of fire (z-axis) and the residual trajectory (line from the origin through P):

$$\lambda = \tan^{-1} \left( \frac{\sqrt{x_o^2 + y_o^2}}{z_o} \right)$$

The Cone Angle is thus a measure of the deflection in trajectory caused by perforation; the orientation of this deflection will be provided by the Phase Angle.

Let  $y_1$  be an arbitrary positive number; let  $r$  be the point  $(0, y_1, z_o)$  and let  $q$  be the point  $(0, 0, z_o)$ . Then the Phase

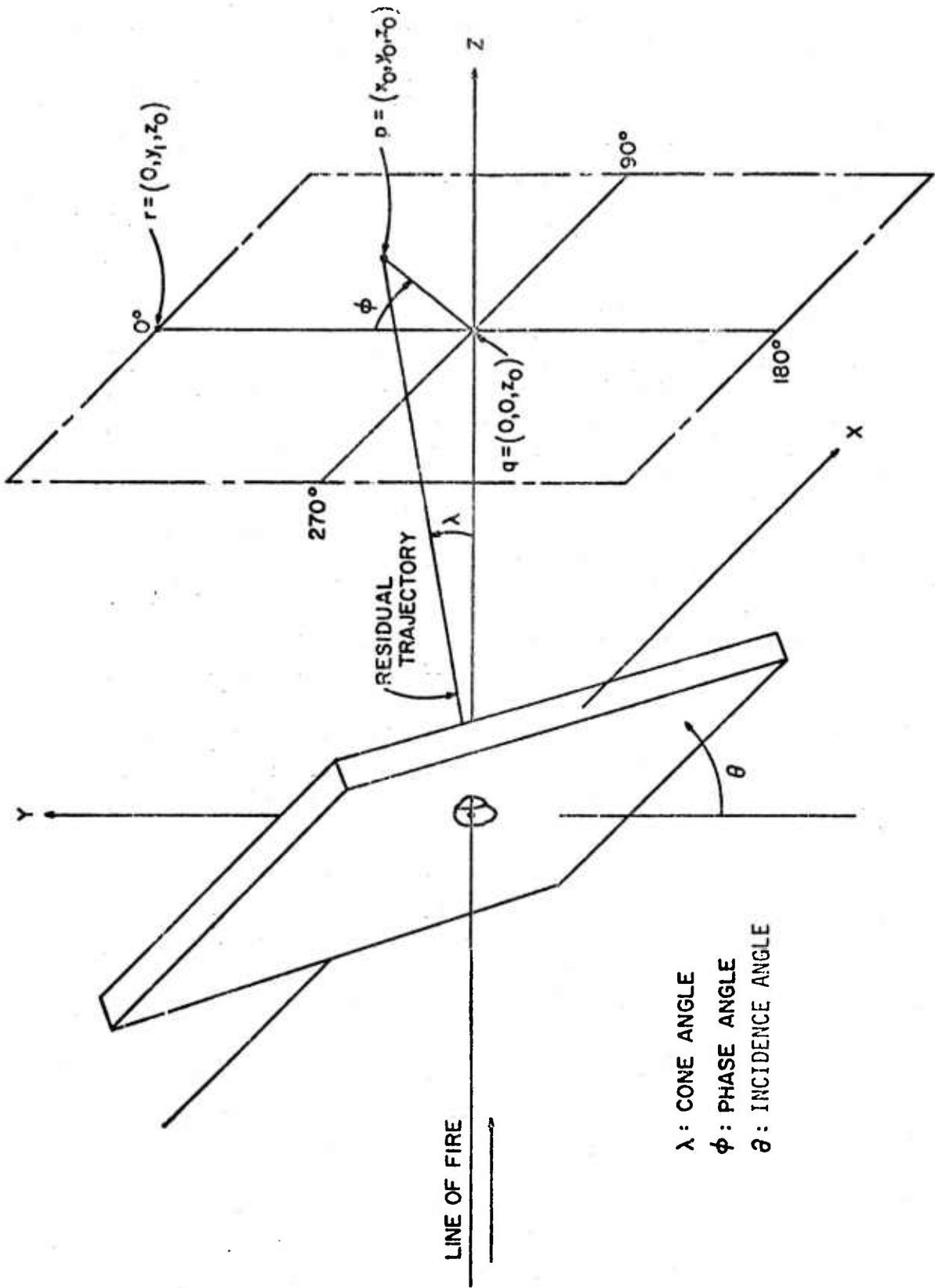


Figure B1. Coordinate System Depicting Angles  $\lambda$ ,  $\phi$ , and  $\theta$

Angle is  $\phi = \angle rqp$  (measured clockwise as perceived from the origin);  $0^\circ \leq \phi < 360^\circ$ . Note that  $\phi$  is not defined if  $\lambda = 0^\circ$ .

We can specify  $\phi$  as follows (for  $\lambda \neq 0^\circ$ ):

$$(i) \text{ If } y_0 = 0, \text{ let } \phi = \begin{cases} 90^\circ & \text{if } x_0 > 0 \\ 270^\circ & \text{if } x_0 < 0 \end{cases}$$

$$(ii) \text{ If } y_0 \neq 0, \text{ let } \psi = \tan^{-1} \left( \frac{x_0}{y_0} \right), \quad -90^\circ < \psi < 90^\circ,$$

$$\text{and } \phi = \begin{cases} \psi + 180^\circ & \text{if } y_0 < 0 \\ \psi & \text{if } y_0 > 0 \text{ and } x_0 \geq 0 \\ \psi + 360^\circ & \text{if } y_0 > 0 \text{ and } x_0 < 0. \end{cases}$$

9. Striking Yaw: Vertical ( $\alpha$ ), Horizontal ( $\beta$ ), Total ( $\delta$ ) - (See Figure B2) for the penetrator at a point prior to impact, let A be the penetrator axis of symmetry; let  $A_1$  and  $A_2$  be the orthogonal projections of A on the y-z (vertical) and x-z (horizontal) planes respectively. The Vertical Striking Yaw,  $\alpha$ , is the acute angle from the penetrator trajectory (initially the line of fire along the z axis) to  $A_1$  (positive orientation being counter-clockwise as seen from the positive x-direction). The Horizontal Striking Yaw,  $\beta$ , is the acute angle from the penetrator trajectory to  $A_2$  (positive orientation being clockwise as seen from the positive y direction). The Total Striking Yaw,  $\delta$ , is the (positive) acute angle between the z-axis and A; in terms of  $\alpha$  and  $\beta$ ,

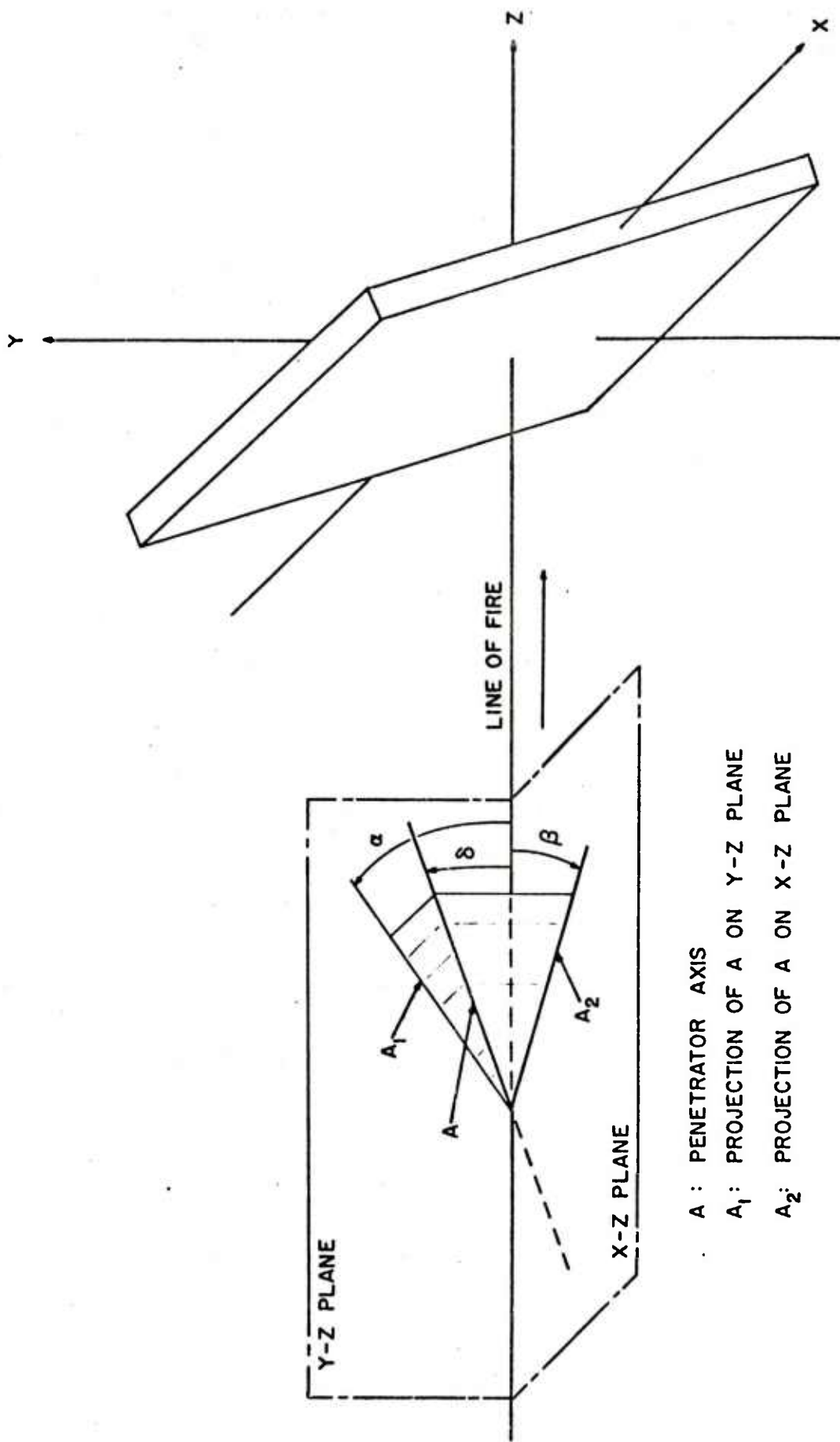
$$\delta = \tan^{-1} \sqrt{\tan^2 \alpha + \tan^2 \beta}.$$

Note i: behind-target vertical, horizontal, and total yaws are defined analogously - reset the coordinate system so that the z-axis coincides with the residual trajectory.

Note ii: total yaw,  $\delta$ , is not generally susceptible to direct measurement; rather its "components"  $\alpha$  and  $\beta$  are inferred from side and bottom radiographic images. Vertical and horizontal striking yaws are properly derived from images at the last radiograph station before the target.

10. Residual Velocity ( $V_r$ ) - zero if the penetrator does not perforate the target; otherwise, the post-perforation velocity (speed) of the residual penetrator (or other piece if so indicated) as determined from the position, time history of behind-target radiographic images.

11. Vertical Yaw Rate - Rate of change, in rev/s, of behind-target vertical yaw.



- A : PENETRATOR AXIS
- A<sub>1</sub> : PROJECTION OF A ON Y-Z PLANE
- A<sub>2</sub> : PROJECTION OF A ON X-Z PLANE

Figure B2. Coordinate System Depicting Yaw Angles  $\alpha$ ,  $\beta$  and  $\delta$

## REFERENCES

1. Gordon R. Johnson, "EPIC-3 A Computer Program for Elastic-Plastic Impact Calculations in 3 Dimensions," BRL CR 343, July 1977. (AD A043281)
2. Gordon R. Johnson, "Further Development of the EPIC-3 Computer Program For Three-Dimensional Analysis of Intense Impulsive Loading," AFATL-TR-78-81, July 1978.
3. J. P. Lambert, "A Residual Velocity Predictive Model for Long Rod Penetrators," ARBRL-MR-02828, September 1977. (AD B027660)
4. J. A. Zukas and B. E. Ringers, "Numerical Simulation of Impact Phenomena," Proceedings of the 1980 Summer Computer Conference, AFIPS Press, 1980.
5. G. H. Jonas and J. A. Zukas, "The Mechanics of Penetration: Analysis and Experiment," Technical Report ARBRL-TR-02137, February 1979.
6. D. Matuska and J. Osborn, to be published. (AD A068463)
7. L. D. Bertholf and M. E. Kipp, et. al., "Kinetic Energy Projectile Impact on Multi-Layered Targets: Two Dimensional Stress Wave Calculations," ARBRL-CR-00391, January 1979. (AD B037370L)
8. Dr. E. Bloore, private communication.
9. Dr. G. Moss, private communication.
10. Dr. D. Curran, private communication.

DISTRIBUTION LIST

| <u>No. of<br/>Copies</u> | <u>Organization</u>   | <u>No. of<br/>Copies</u> | <u>Organization</u>  |
|--------------------------|---|--------------------------|--|
| 12                       | Commander<br>Defense Technical Info Center<br>ATTN: DDC-DDA<br>Cameron Station<br>Alexandria, VA 22314                                  | 1                        | Commander<br>US Army Electronics Research<br>and Development Command<br>Technical Support Activity<br>ATTN: DELSD-L<br>Fort Monmouth, NJ 07703   |
| 1                        | Commander<br>US Army Materiel Development<br>and Readiness Command<br>ATTN: DRCDMD-ST<br>5001 Eisenhower Avenue<br>Alexandria, VA 22333 | 2                        | Commander<br>US Army Missile Command<br>ATTN: DRSMI-R<br>DRSMI-YDL<br>Redstone Arsenal, AL 35809   |
| 2                        | Commander<br>US Army Armament Research<br>and Development Command<br>ATTN: DRDAR-TSS<br>Dover, NJ 07801                                 | 1                        | Commander<br>US Army Tank-Automotive Rsch<br>and Development Command<br>ATTN: DRDTA-UL<br>Warren, MI 48090   |
| 1                        | Commander<br>US Army Armament Materiel<br>Readiness Command<br>ATTN: DRSAR-LEP-L, Tech Lib<br>Rock Island, IL 61299                     | 1                        | Director<br>US Army TRADOC Systems<br>Analysis Activity<br>ATTN: ATAA-SL, Tech Lib<br>White Sands Missile Range<br>NM 88002  |
| 1                        | Director<br>US Army ARRADCOM<br>Benet Weapons Laboratory<br>ATTN: DRDAR-LCB-TL<br>Watervliet, NY 12189                                  | 1                        | Commander<br>Fleet Marine Force, Atlantic<br>ATTN: G-4 (NSAP)<br>Norfolk, VA 23511   |
| 1                        | Commander<br>US Army Aviation Research<br>and Development Command<br>ATTN: DRDAV-E<br>4300 Goodfellow Blvd.<br>St. Louis, MO 61320      |                          | <u>Aberdeen Proving Ground</u><br>Dir, USAMSAA<br>ATTN: DRXSY-D<br>DRXSY-MP, H. Cohen<br>Cdr, USATECOM<br>ATTN: DRSTE-TO-F<br>Director, USACSL<br>Bldg E3516, EA<br>ATTN: DRDAR-CLB-PA |
| 1                        | Director<br>US Army Air Mobility Research<br>and Development Laboratory<br>Ames Research Center<br>Moffett Field, CA 94035              |                          |  |
| 1                        | Commander<br>US Army Communications Rsch<br>and Development Command<br>ATTN: DRDCO-PPA-SA<br>Fort Monmouth, NJ 07703                    |                          |  |

USER EVALUATION OF REPORT

Please take a few minutes to answer the questions below; tear out this sheet, fold as indicated, staple or tape closed, and place in the mail. Your comments will provide us with information for improving future reports.

1. BRL Report Number \_\_\_\_\_

2. Does this report satisfy a need? (Comment on purpose, related project, or other area of interest for which report will be used.)

\_\_\_\_\_  
\_\_\_\_\_  
\_\_\_\_\_

3. How, specifically, is the report being used? (Information source, design data or procedure, management procedure, source of ideas, etc.) \_\_\_\_\_

\_\_\_\_\_  
\_\_\_\_\_

4. Has the information in this report led to any quantitative savings as far as man-hours/contract dollars saved, operating costs avoided, efficiencies achieved, etc.? If so, please elaborate.

\_\_\_\_\_  
\_\_\_\_\_

5. General Comments (Indicate what you think should be changed to make this report and future reports of this type more responsive to your needs, more usable, improve readability, etc.) \_\_\_\_\_

\_\_\_\_\_  
\_\_\_\_\_  
\_\_\_\_\_

6. If you would like to be contacted by the personnel who prepared this report to raise specific questions or discuss the topic, please fill in the following information.

Name: \_\_\_\_\_

Telephone Number: \_\_\_\_\_

Organization Address: \_\_\_\_\_

\_\_\_\_\_  
\_\_\_\_\_